

# A Study of Ductile Damage and Failure of Pure Copper – Part I: Constitutive Equations and Experiments

M. Zapara, N. Tutyshkin, W.H. Müller, R. Wille

*This paper presents the results of an experimental study of ductile damage and failure of pure copper. Uniaxial tension tests were performed for specimens with different arrangements of pre-drilled micro-holes representing the simulation models of cylindrical voids. This experimental method has already been applied by a number of researchers in order to investigate the damage of metals under plastic deformation and proved to be useful for studying an evolution of damage in ductile materials in terms of local strains of both representative volume elements (RVE) and meso-elements (i.e., material unit cells with a single void). Two measures are used for the assessment of damage in the deformed material. The first one relates damage to an increase in the void volume. The second measure accounts for the damage associated with a change in the void shape. Both measures were introduced as part of a tensorial theory of damage in Zapara et al. (2008). They are based on experimental studies of damage kinetics in metallic materials under plasticity conditions. In combination with similar data from the literature the obtained results are important for the modeling of metal forming processes with dominating tensile deformation (e.g., deep-drawing, ironing, wire drawing).*

## 1 Introduction

Damage of metals subjected to plastic deformation is mainly governed by void nucleation and growth (Yokobori, 1968). McClintock (1968) was the first to recognize the role of microvoids in ductile failure processes and tried to correlate the mean radius of nucleated cavities to the overall plastic strain increment. Rice and Tracey (1969) studied the evolution of spherical voids in an elastic-perfectly plastic matrix analytically. In these pioneering investigations the interaction between microvoids, the coalescence process, and hardening effects were neglected, and failure was postulated to occur when the cavity radius would reach a critical value specific for the material. Fleck and Hutchinson (1986) expanded these results and, for the first time, led to the clarification of void growth and void shape evolution in shear bands. However, their approach was restricted to an isolated void in an infinite matrix material. It is well known that void coalescence followed by the formation of large cavities occurs in the direction of shear bands, especially under large deformations (*cf.*, *e.g.*, Yokobori, 1968). In turn these cavities can be sources of localized strain bands. In order to illustrate the void interaction we may introduce besides the RVE (Fig. 1) a meso-element, which represents the material unit cell with a single void (Fig. 2) (for more details on the geometrical representation see Zapara *et al.*, 2008). The void volume fraction will be used as an internal parameter:  $f_v = \Delta V_v / \Delta V_{RVE}$ , where  $\Delta V_v$  denotes the volume occupied by voids within the RVE of size  $\Delta V_{RVE}$ .

Based on this method further pioneering work was undertaken by Gurson (1977) who obtained constitutive models for solids containing circular-cylindrical or spherical voids through an upper bound approach. Other studies involving such methods were presented by Tracey (1971) and Needleman (1972) who modeled the response of an array of circular-cylindrical voids, and by Licht and Suquet (1988) who gave a simple model for cylindrical void growth in a non-linearly viscous material at arbitrary void volume fractions. The Gurson model is widely used for the analysis of ductile failure phenomena. When applied there is a non-uniqueness problem in determining the Gurson parameters and linking them to material properties. Needleman and Tvergaard (1984) and Koplik and Needleman (1988) extended the initial formulation proposed by Gurson in order to include the acceleration in the failure process induced by void coalescence. Zhang and Hauge (1990) classified the parameters involved in the Gurson model into strain gradient-sensitive and -insensitive parameters. A physical mechanism based failure criterion for void coalescence was implemented in their paper, resulting in a complete Gurson model. The critical void volume fraction at void coa-

lescence was assumed to be a material specific response, which in general depends on the stress state. The void volume fraction was postulated to depend on the distribution of void nucleation.

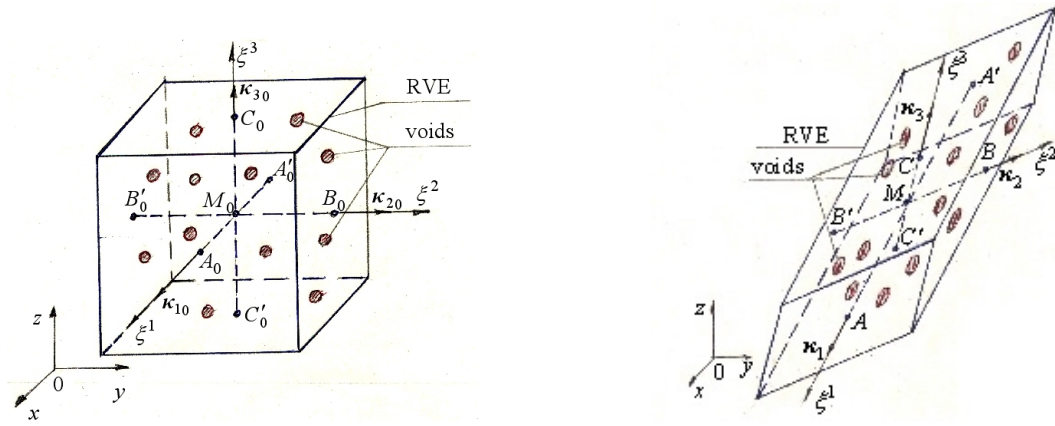


Figure 1. Representative volume element (RVE) under arbitrarily complex deformation: *left* initial moment, *right* current moment

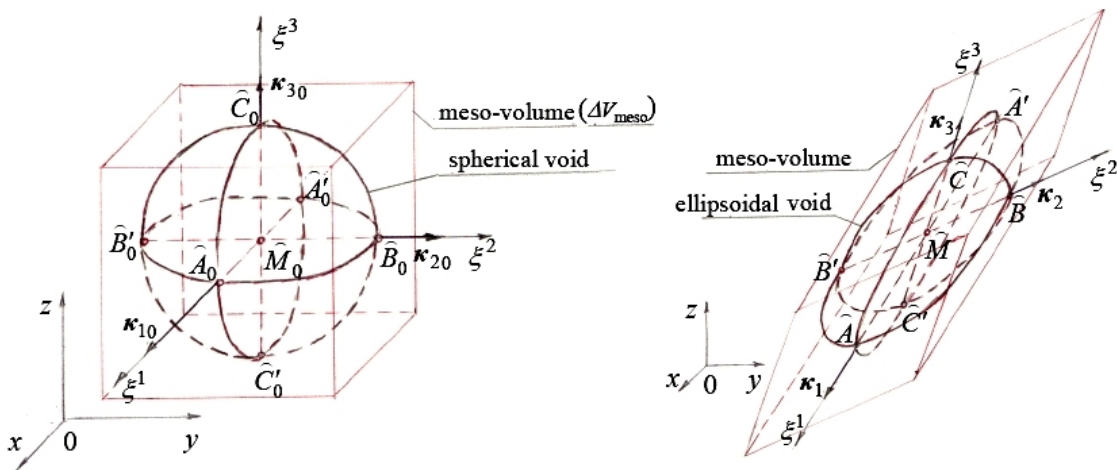


Figure 2. Meso-element with an ellipsoidal void under arbitrarily complex deformation: *left* initial moment, *right* current moment

Gologanu *et al.* (1993) extended the classical Gurson analysis of a hollow rigid ideal-plastic sphere loaded axisymmetrically to an ellipsoidal volume containing a confocal ellipsoidal cavity in order to define approximate models for ductile metals containing non-spherical voids. Moreover in Gologanu *et al.* (2001 a,b) theoretical models for void coalescence in porous ductile solids were developed. The authors considered a cylindrical RVE containing an initially spheroidal void subjected to some axisymmetric loading. In a first case study the major stress applied is an axial one so that voids gradually concentrate in horizontal bands and coalesce due to a sudden concentration of the deformation in these regions. In the second case study the major stress applied is of lateral nature so that voids gradually concentrate along vertical columns and gradually coalesce. Comparison of the model predictions with the FE results exhibits a good agreement for a wide range of triaxialities. Tvergaard and Niordson (2004) investigated the role of smaller size voids in a ductile damage material by using a local plasticity model as proposed by Acharya and Bassani (2000). Schacht *et al.* (2003) used a 3D unit cell with voids to investigate the role and the effects associated with the crystallographic orientation of the matrix material, finding a substantial dependency of the growth and coalescence phase with the anisotropy of the material surrounding the voids.

The important role of the volume growth of the voids as an important factor for the assessment of damage of plastically deformable metals is unquestioned (*cf.*, *e.g.*, Makarov *et al.*, 2007). Nevertheless it seems also necessary to take the influence of the shape of the defects and their direction into account in order to study the evolution of the strain damage in more detail (*cf.*, *e.g.*, Horstemeyer *et al.*, 2000; Klöcker and Tvergaard, 2003). Voids assume a prolate (or oblate, depending on the stress state) ellipsoidal shape under large plastic deformation. At the same time it turns out that a spatial orientation of the principal axes of the meso-ellipsoid is related to the directions of the principal strains  $\varepsilon_1, \varepsilon_2, \varepsilon_3$  of the material particle containing a void (*i.e.*, a meso-element, *cf.*, Fig. 2).

Under complex (non-uniform) loading the ratio between the principal strains  $\varepsilon_1, \varepsilon_2, \varepsilon_3$  changes and the principal strain axes rotate over the material fibers (*i.e.*, w.r.t an accompanying coordinate system). At the initial moment of the deformation the shape of the particle meso-volume is a cube, and the void shape is a sphere (with the volume  $\Delta V_{v0}$ ). The space orientation of the meso-parallelepiped corresponds to an accompanying coordinate system  $\xi^k$ ,  $k = 1, 2, 3$ , chosen at the initial moment  $t_0$  (*cf.*, Fig. 2, left). The accompanying axes  $\xi^k$  are rigidly connected with the particles of the continuum and deform concurrently. Therefore, the accompanying Cartesian system of orthogonal coordinates chosen at the initial moment becomes, generally speaking, curvilinear and non-orthogonal under arbitrarily complex deformation. During arbitrarily complex deformation (for the finite period  $\Delta t = t - t_0$ ) the cube-shaped meso-volume transforms into an oblique parallelepiped, and the spherical void transforms into an ellipsoid of volume  $\Delta V_v$ . Geometrical models of the RVE and the meso-element allow us to determine the characteristics of deformation appearing in the constitutive equations for strain-induced damage.

Metals are characterized by a tensor of strain-induced damage. That is why a number of the authors (*cf.*, *e.g.*, Menzel and Steinmann, 2001; Brünig, 2003; Lemaitre and Desmorat, 2007; Hammi and Horstemeyer, 2007) use a damage tensor when studying processes with plastic deformation. The theory of Thomason (1990) assumes that the material deforms homogeneously until localized deformation between the voids intervenes. The fracture is expected to occur so rapidly after the onset of localized deformation that the transition from homogeneous to inhomogeneous deformation is used as a criterion for ductility. In the Thomason model it is assumed that coalescence results by reaching a state of plastic limit load inducing failure of the intervoid matrix. By assuming axial symmetry and ellipsoidal void growth Thomason formulated the condition for the onset of void coalescence.

Pardoen *et al.* (1998) analyzed available criteria of void coalescence in view of void shape change. They performed tensile tests using notched round copper bars. The metallographic study showed that coalescence always occurred in the narrowest section of the specimen. The crucial result of this experimental study of damage kinetics consisted in confirming that coalescence evolves from a microscopic localization of plastic shear within very small bands of the material. This fact proves the known analytical criterion for the onset of void coalescence developed by Brown and Embury (1974). This criterion can be interpreted from an explicit micro-mechanical point of view: In a perfectly plastic material the formation of micro-shear bands (directed mainly at  $45^\circ$  to the tensile load), which connect two voids, will lead rapidly to the fracture of the ligament. From geometrical arguments, this criterion can be generalized for any pair of ellipsoidal voids. The published results have a significant practical value for the modeling of ductile damage in processes with multiaxial stress states. Bonora *et al.* (2005) have shown a possibility to predict elastic failure of metals in such processes by using damage parameters that were determined experimentally in simple uniaxial tests.

In our experiments we study the evolution of damage depending on the local strains of both RVE and meso-elements with artificial voids (*viz.*, pre-machined holes). This technique was initially applied by Tait and Taplin (1979). The plastic deformation of specimens with artificial defects has been investigated later by a number of authors in order to understand the evolution of damage (*cf.*, *e.g.* Magnusen *et al.*, 1988; Dung, 1992; Kannan and Hamilton, 1998; Khraishi *et al.*, 2001; Mulholland *et al.*, 2006; Zapara *et al.*, 2010). The recent publications by Weck and Wilkinson (2008) and Weck *et al.* (2008) presented remarkable results by using this approach. They showed the importance of void spacing and orientation for void coalescence. Controlled visualization of void growth and coalescence in model materials containing laser-drilled holes allowed them to describe damage and failure mechanisms accurately which are difficult to obtain experimentally because of the stochastic nature of void coalescence, the considerable number of voids, and the difficulty of observing voids inside the sample.

In our paper this method is applied to the experimental research and modeling of strain-induced damage for pure copper under large tensile deformations typical for deep-drawing operations. In the next section we will briefly present the constitutive equations for strain induced damage of metals. Then we will explain the problem and the corresponding experimental study, and describe how the tests were performed (Section 3). This will then be followed by experimental results (Section 4). We conclude with a discussion (Section 5).

## 2 Constitutive Equations for Strain Induced Damage

Plastic strains in deformed metals amount to 70...90%, *i.e.*, they are approximately a hundred times larger than the elastic strains occurring in metal forming processes, such as drawing, press forging, and extrusion. Therefore the constitutive equations include only the plastic strains. The tensors of strain increments and strain rates can be written as  $d\boldsymbol{\varepsilon} = d\boldsymbol{\varepsilon}^p$  and  $\dot{\boldsymbol{\varepsilon}} = \dot{\boldsymbol{\varepsilon}}^p$ , respectively. The appropriateness of a rigid-plastic material model during the analysis of metal forming processes was demonstrated by Hill (1950), Prager and Hodge (1951), Kachanov (2004), *etc.* Analogously to the determination of the strains at the RVE-level and meso-level we introduce the tensors of strain increments and strain rates at the RVE-level:  $d\boldsymbol{\varepsilon}$  and  $\dot{\boldsymbol{\varepsilon}}$  and at the meso-level:  $d\bar{\boldsymbol{\varepsilon}}$  and  $\dot{\bar{\boldsymbol{\varepsilon}}}$ , respectively. The corresponding tensorial components are denoted as follows:  $d\varepsilon_{ij}$ ,  $\dot{\varepsilon}_{ij}$ ,  $d\bar{\varepsilon}_{ij}$ ,  $\dot{\bar{\varepsilon}}_{ij}$ , including volumetric parts:  $d\varepsilon_{kk}$ ,  $\dot{\varepsilon}_{kk}$ ,  $d\bar{\varepsilon}_{kk}$ ,  $\dot{\bar{\varepsilon}}_{kk}$ , and deviatoric components:  $de_{ij}$ ,  $\dot{e}_{ij}$ ,  $d\bar{e}_{ij}$ ,  $\dot{\bar{e}}_{ij}$ , as well as the equivalent von Mises measures:  $d\varepsilon_{eq}$ ,  $\dot{\varepsilon}_{eq}$ ,  $\varepsilon_{eq}$ ,  $d\bar{\varepsilon}_{eq}$ ,  $\dot{\bar{\varepsilon}}_{eq}$ ,  $\bar{\varepsilon}_{eq}$ .

In order to study forming processes (with large finite deformations) in combination with damage analysis, *i.e.*, with the analysis of a change in volume and shape of defects at the meso-level, it is reasonable to use a symmetric second order damage rate tensor  $\dot{\boldsymbol{\omega}}$  (*cf.*, Zapara *et al.*, 2008). The constitutive equations for the internal variables ( $\dot{e}_{ij}$ ,  $\dot{r}$ ,  $\dot{\omega}_{ij}$ ) can be derived from a dissipation potential  $F$ , which is a convex function of the associated variables ( $-s_{ij}$ ,  $R$ ,  $-Y_{ij}$ ). The convexity of the dissipation potential in an associated variable space follows from the second principle of thermodynamics, *i.e.*, the CLAUSIUS-DUHEM inequality (*cf.*, *e.g.*, Collins and Houlsby, 1997; Houlsby and Puzrin, 2000; Brüning, 2003; Voyiadjis and Dorgan, 2007; Einav *et al.*, 2007; Stumpf *et al.*, 2009). Thus, we find:

$$\dot{e}_{ij} = \dot{\lambda} \frac{\partial F}{\partial s_{ij}}, \quad \dot{r} = -\dot{\lambda} \frac{\partial F}{\partial R}, \quad \dot{\omega}_{ij} = \dot{\lambda} \frac{\partial F}{\partial Y_{ij}}. \quad (1)$$

where  $\dot{e}_{ij}$  are the deviatoric plastic strain rates (at the RVE-level),  $\dot{r}$  is the isotropic hardening parameter,  $\dot{\omega}_{ij}$  are the components of the damage rate tensor  $\dot{\boldsymbol{\omega}}$ ,  $s_{ij}$  are the deviatoric stresses,  $R$  is the isotropic hardening stress parameter,  $Y_{ij}$  are the components of the tensor  $\mathbf{Y}$  which accounts for the energy density release rate related to the void growth and a change in its shape, and  $\dot{\lambda}$  is the plastic Lagrange multiplier.

In view of the published qualitative experiments (Bonora *et al.*, 2005; Lemaitre and Desmorat, 2007) we can decompose the potential  $F$  as the sum:

$$F = \Phi + \Omega \quad (2)$$

where  $\Phi$  and  $\Omega$  refer to the plastic potential and the damage potential, respectively.

In view of Eq. (2) Eqs. (1) assume the following form:

$$\dot{e}_{ij} = \dot{\lambda} \frac{\partial \Phi}{\partial s_{ij}}, \quad \dot{r} = -\dot{\lambda} \frac{\partial \Phi}{\partial R}, \quad \dot{\omega}_{ij} = \dot{\lambda} \frac{\partial \Omega}{\partial Y_{ij}}. \quad (3)$$

Following Kachanov (2004) the von Mises yield function  $f$  can be used as a plastic potential  $\Phi$ :

$$f(s_{ij}, R) = (1/2)s_{ij}s_{ij} - \tau_y^2 = 0, \quad (4)$$

where  $\tau_y$  is the yield stress under shear.

The plastic multiplier  $\dot{\lambda}$  is proportional to the plastic strain energy density rate,  $\dot{w}_p$  :

$$\dot{w}_p = s_{ij}\dot{e}_{ij} = \dot{\lambda}s_{ij}s_{ij} = \frac{2}{3}\dot{\lambda}\sigma_{eq}^2, \quad (5)$$

Eq. (5) results in:

$$\dot{\lambda} = \frac{3}{2} \frac{\dot{w}_p}{\sigma_{eq}^2} = \frac{3}{2} \frac{s_{ij}\dot{e}_{ij}}{\sigma_{eq}^2} = \frac{3}{2} \frac{\dot{e}_{ij}\dot{e}_{ij}}{\dot{\lambda}\sigma_{eq}^2} = \frac{9}{4} \frac{\dot{\epsilon}_{eq}^2}{\dot{\lambda}\sigma_{eq}^2}, \quad (6)$$

where  $\sigma_{eq}$  and  $\dot{\epsilon}_{eq} = \sqrt{(2/3)\dot{e}_{ij}\dot{e}_{ij}}$  denote the equivalent von Mises stress and strain rate (both related to the RVE), respectively. In view that  $\sigma_{eq} = \tau_y \sqrt{3}$  (at the yield state) we may finally write:

$$\dot{\lambda} = \frac{\sqrt{3}}{2} \frac{\dot{\epsilon}_{eq}}{\tau_y}, \quad (7)$$

When calculating stresses and strains we will consider isotropic hardening that is typical for large plastic deformations at metal forming. The conjugate force of isotropic hardening is the stress parameter  $R = \sqrt{(1/2)s_{ij}s_{ij}} = \tau_y$ , which describes a change in the radius of the von Mises cylinder (4) in the principal stress space  $\sigma_1, \sigma_2, \sigma_3$ . The isotropic hardening parameter,  $\dot{r}$ , can be written as follows:

$$\dot{r} = -\dot{\lambda} \frac{\partial [(1/2)s_{ij}s_{ij} - \tau_y^2]}{\partial (\tau_y)} = 2\dot{\lambda}\tau_y = \dot{\epsilon}_{eq}\sqrt{3}. \quad (8)$$

The damage potential  $\Omega$  for a rigid-plastic material model can be defined as a quadratic function of the first invariant  $I_1(\dot{\bar{\epsilon}})$  of the strain rate tensor  $\dot{\bar{\epsilon}}$  for meso-elements and the linear function of the second invariant  $I_2(\dot{\bar{\epsilon}})$  of the deviatoric strain rate tensor  $\dot{\bar{e}}$  for meso-elements:

$$\Omega = \frac{1}{\lambda^2} \left( \frac{1}{6} (\dot{\bar{\epsilon}}_{kk})^2 + \frac{1}{2} \dot{\bar{e}}_{ij}\dot{\bar{e}}_{ij} \right) = \frac{1}{\lambda^2} \left( \frac{1}{6} I_1^2(\dot{\bar{\epsilon}}) + I_2(\dot{\bar{\epsilon}}) \right). \quad (9)$$

Eq. (9) can be interpreted in terms of energy: The first term in brackets, which includes the function  $\frac{1}{6} (\dot{\bar{\epsilon}}_{kk})^2$ , defines the dissipation related to plastic dilatation caused by the growth of the void volume. The second term, which includes the invariant  $\frac{1}{2} \dot{\bar{e}}_{ij}\dot{\bar{e}}_{ij}$ , accounts for the dissipation related to a change in the meso-element shape.

The tensor  $Y$  can be defined by the linear function of the strain rate tensor for meso-elements.

$$Y_{ij} = k_Y \frac{1}{\lambda} \dot{\bar{\epsilon}}_{ij}. \quad (10)$$

As a normalizing factor  $k_Y$  we may use the following integral quantity  $\bar{\epsilon}_f$  (to the moment  $t_f$  of macroscopic failure):

$$k_Y = \bar{\epsilon}_f = \int_{t_f} \sqrt{6\dot{\lambda}\Omega^{1/2}} dt = \int_{t_f} \sqrt{3} \left( \frac{1}{3} I_1^2(\dot{\bar{\epsilon}}) + 2I_2(\dot{\bar{\epsilon}}) \right)^{1/2} dt = \int_{t_f} \left( (\dot{\bar{\epsilon}}_{kk})^2 + 3\dot{\bar{e}}_{ij}\dot{\bar{e}}_{ij} \right)^{1/2} dt = \int_{t_f} \left( (\dot{\bar{\epsilon}}_{kk})^2 + \frac{9}{2} \dot{\bar{\epsilon}}_{eq}^2 \right)^{1/2} dt. \quad (11)$$

In view of Eqs. (10) and (11) Eq. (9) becomes:

$$\Omega = \frac{1}{\bar{\varepsilon}_f^2} \left( \frac{1}{6} (Y_{kk})^2 + \frac{1}{2} \tilde{Y}_{ij} \tilde{Y}_{ij} \right) = \frac{1}{\bar{\varepsilon}_f^2} \left( \frac{1}{6} I_1^2(\mathbf{Y}) + I_2(\tilde{\mathbf{Y}}) \right), \quad (12)$$

where  $Y_{kk}$  and  $\tilde{Y}_{ij}$  are the volumetric and deviatoric components of the tensor  $\mathbf{Y}$ .

The damage potential (12) in view of Eq. (3)<sub>3</sub>, defines the damage rate tensor  $\dot{\omega}$ :

$$\dot{\omega}_{ij} = \dot{\lambda} \frac{\partial \Omega}{\partial Y_{ij}} = \frac{\dot{\lambda}}{\bar{\varepsilon}_f^2} Y_{ij}, \quad (13)$$

or, taking Eq. (10) into account, we have:

$$\dot{\omega}_{ij} = \frac{\dot{\bar{\varepsilon}}_{ij}}{\bar{\varepsilon}_f}, \quad (14)$$

Following the summation rule for repetitive indices  $i, j, k = 1, 2, 3$ , we may rewrite Eq. (12) with the invariants in detail:

$$\begin{aligned} \Omega &= \frac{1}{\bar{\varepsilon}_f^2} \left( \frac{1}{6} (Y_{11} + Y_{22} + Y_{33})^2 - \tilde{Y}_{11} \tilde{Y}_{22} - \tilde{Y}_{22} \tilde{Y}_{33} - \tilde{Y}_{33} \tilde{Y}_{11} + \tilde{Y}_{12}^2 + \tilde{Y}_{23}^2 + \tilde{Y}_{31}^2 \right) = \\ &= \frac{1}{\bar{\varepsilon}_f^2} \left( \frac{1}{6} (Y_{11} + Y_{22} + Y_{33})^2 + \frac{1}{6} \left( (Y_{11} - Y_{22})^2 + (Y_{22} - Y_{33})^2 + (Y_{33} - Y_{11})^2 \right) + Y_{12}^2 + Y_{23}^2 + Y_{31}^2 \right). \end{aligned} \quad (15)$$

Using the principal axes 1, 2, 3 of the tensor  $\mathbf{Y}$  instead of the axes  $x_i$  (with  $i = 1, 2, 3$ ) we may rewrite Eq. (15) as follows:

$$\Omega(Y_{ij}) = \frac{1}{2\bar{\varepsilon}_f^2} \left( (Y_1)^2 + (Y_2)^2 + (Y_3)^2 \right), \quad (16)$$

This dependence can be represented in the space of principal components  $(Y_1, Y_2, Y_3)$  by a spherical surface with the radius  $\bar{\varepsilon}_f \sqrt{2\Omega(Y_{ij})}$  whose center coincides with the origin of coordinates. The damage increments  $(d\omega_{ij} = \dot{\omega}_{ij} dt)$  can be represented in the spaces  $Y_{ij}$  and  $\tilde{\varepsilon}_{ij}$  by a vector if we multiply the components  $d\omega_{ij}$  by an equidimensional constant. Since the direction cosines of the normal to the potential surface  $\Omega = \text{const}$  in the spaces  $Y_{ij}$  and  $\tilde{\varepsilon}_{ij}$  are proportional to the derivatives  $\partial\Omega/\partial Y_{ij}$  and  $\partial\Omega/\partial \tilde{\varepsilon}_{ij}$  the vector  $d\omega_{ij}$  coincides with the outer normal to the damage potential surface according to Eq. (3)<sub>3</sub>.

A decomposition of the increments of the damage tensor  $d\omega$  into a volumetric and a deviatoric part,  $d\omega_{ij} = (1/3)\delta_{ij} d\omega_{kk} + d\tilde{\omega}_{ij}$  (where  $d\omega_{kk}$  denotes the first invariant of the tensor  $d\omega$  and  $\delta_{ij}$  is the Kronecker delta), is physically meaningful. The volumetric part,  $(1/3)\delta_{ij} d\omega_{kk}$ , describes the damage increment caused by a change in the volume of the void. The deviatoric increment,  $d\tilde{\omega}_{ij}$ , accounts for the increase in damage caused by a change in void shape. Such a view on damage kinetics enables us to introduce two damage measures,  $\omega_1$  and  $\omega_2$ , for damage assessment (*cf.*, Zapara *et al.*, 2008):

$$d\omega_1 = d\omega_{kk} = \frac{\dot{\bar{\varepsilon}}_{kk}}{\bar{\varepsilon}_f} dt, \quad d\omega_2 = \sqrt{3\tilde{\omega}_{ij}\tilde{\omega}_{ij}} dt = \frac{\sqrt{3\dot{\bar{\varepsilon}}_{ij}\dot{\bar{\varepsilon}}_{ij}}}{\bar{\varepsilon}_f} dt = \frac{3}{\sqrt{2}} \frac{\dot{\bar{\varepsilon}}_{\text{eq}}}{\bar{\varepsilon}_f} dt, \quad (17)$$

We may represent Eq. (11) in terms of strain increments:

$$\bar{\varepsilon}_f = \int_{t_f} \left( \left( \dot{\bar{\varepsilon}}_{kk} \right)^2 + \frac{9}{2} \dot{\bar{\varepsilon}}_{eq}^2 \right)^{1/2} dt = \int_{t_f} \dot{\zeta} dt = \int_{\zeta_f} d\zeta, \quad \dot{\zeta} = \left( \left( \dot{\bar{\varepsilon}}_{kk} \right)^2 + \frac{9}{2} \dot{\bar{\varepsilon}}_{eq}^2 \right)^{1/2}. \quad (18)$$

Fig. 3 (left) shows a mapping plane with Cartesian rectangular coordinates:  $\xi = \bar{\varepsilon}_{kk}$ ,  $\eta = (3/\sqrt{2})\bar{\varepsilon}_{eq}$ , where  $\xi, \eta \in [0; \infty]$ . The integral value of  $\bar{\varepsilon}_f$  can be defined by the length of the arc  $O\zeta_f$ :  $\bar{\varepsilon}_f = \int_{\zeta_f} d\zeta$ , where the point  $\zeta_f$  corresponds to the moment of macroscopic failure. In case of a proportional increase in plastic dilatation  $\bar{\varepsilon}_{kk}$  and the equivalent strain  $\bar{\varepsilon}_{eq}$  of meso-elements,  $\bar{\varepsilon}_f$  can be defined by a scalar of the vector  $\overrightarrow{O\zeta_f}$ :  $\bar{\varepsilon}_f = \int_{\zeta_f} d\zeta = \left| \overrightarrow{O\zeta_f} \right|$ . Phase angles of the vectors of failure,  $\overrightarrow{O\zeta_f}$ , and of coalescence,  $\overrightarrow{O\zeta_c}$ , are denoted by  $\vartheta_f = \tan^{-1}\left(\frac{(3/\sqrt{2})\bar{\varepsilon}_{eqf}}{\bar{\varepsilon}_{kkf}}\right)$  and  $\vartheta_c = \tan^{-1}\left(\frac{(3/\sqrt{2})\bar{\varepsilon}_{eqc}}{\bar{\varepsilon}_{kkc}}\right)$ , respectively.

In view of Eqs. (17) the integral normalized measures of damage ( $\omega_1, \omega_2 \in [0; 1]$ ) can be written as follows

$$\omega_1 = \int_t \frac{\dot{\bar{\varepsilon}}_{kk}}{\bar{\varepsilon}_f} dt = \int_{\bar{\varepsilon}_{kk}} \frac{d\bar{\varepsilon}_{kk}}{\bar{\varepsilon}_f}, \quad \omega_2 = \int_t \frac{\sqrt{3\dot{\bar{\varepsilon}}_{ij}\dot{\bar{\varepsilon}}_{ij}}}{\bar{\varepsilon}_f} dt = \int_t \frac{(3/\sqrt{2})\dot{\bar{\varepsilon}}_{eq}}{\bar{\varepsilon}_f} dt = \int_{\bar{\varepsilon}_{eq}} \frac{3\sqrt{2}}{\bar{\varepsilon}_f} d\bar{\varepsilon}_{eq}. \quad (19)$$

Fig. 3 (right) shows a plane of the normalized parameters  $\omega_1$  and  $\omega_2$ . The evolution of damage from the initial state to the failure is represented by the trajectory  $OM_cM_f$ , where the point  $M_c$  corresponds to the onset of void coalescence. This interpretation of damage accumulation allows us to formulate a working hypothesis about the failure locus  $S_f(\omega_1, \omega_2)$  (cf., Fig. 3, right). The locus point  $S_f(1, 0)$  corresponds to failure as a result of critical plastic dilatation but without any change in void shape while the locus point  $S_f(0, 1)$  corresponds to the failure as a result of the critical equivalent strain of the meso-elements containing prolate ellipsoidal voids without any change in their volume. The failure locus  $S_f(\omega_1, \omega_2)$  can be approximated by the Lamé curve:  $\omega_1^b + \omega_2^b = 1$ . Orientations of the failure vector  $\overrightarrow{OM_f}$  and the coalescence vector  $\overrightarrow{OM_c}$  are defined by phase angles  $\nu_f$  and  $\nu_c$ , respectively.

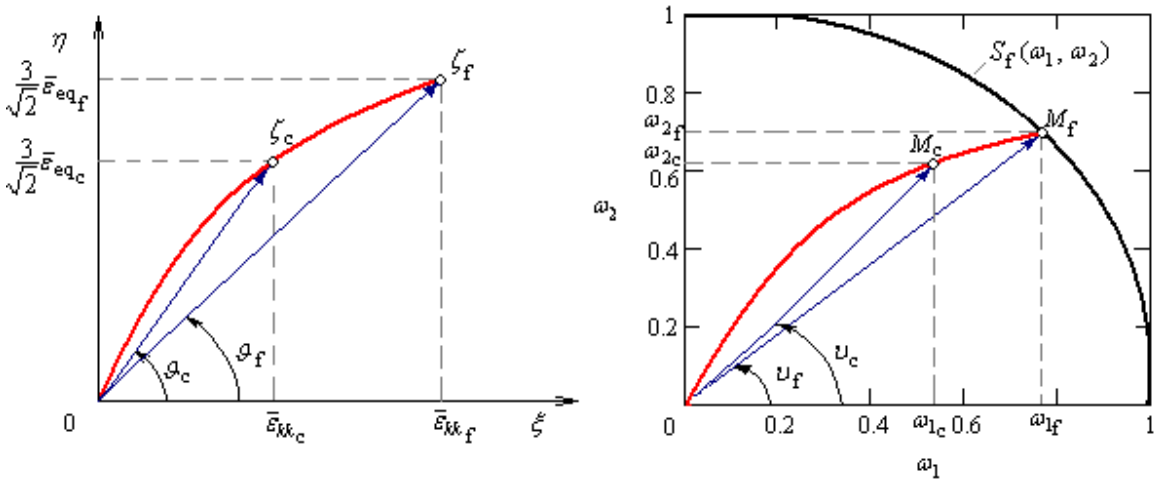


Figure 3. Representation of the evolution of ductile damage:

left – in a plane of  $\eta = \bar{\varepsilon}_{kk}$  and  $\xi = (3/\sqrt{2})\bar{\varepsilon}_{eq}$ ; right – in a plane of  $\omega_2$  and  $\omega_1$

The theoretical framework given above is an extension of the damage theory presented by Kachanov (1986). If one neglects the change in void shape Eqs. (3)<sub>3</sub> and (9) - (14) become:

$$\begin{aligned}\dot{\omega}_{kk} &= \dot{\lambda} \frac{\partial \Omega}{\partial Y_{kk}}, \quad k_Y = \bar{\varepsilon}_f = \int_{t_f} \dot{\bar{\varepsilon}}_{kk} dt = \bar{\varepsilon}_{kkf}, \quad Y_{kk} = k_Y \frac{1}{\dot{\lambda}} \dot{\bar{\varepsilon}}_{kk} = \frac{\bar{\varepsilon}_{kkf}}{\dot{\lambda}} \dot{\bar{\varepsilon}}_{kk}, \\ \Omega &= \frac{1}{6\dot{\lambda}^2} (\dot{\bar{\varepsilon}}_{kk})^2 = \frac{1}{6\dot{\lambda}^2} I_2(\dot{\bar{\boldsymbol{\varepsilon}}}) = \frac{1}{6(\bar{\varepsilon}_{kkf})^2} (Y_{kk})^2 = \frac{1}{6(\bar{\varepsilon}_{kkf})^2} I_1^2(\mathbf{Y}) = \frac{1}{6(\bar{\varepsilon}_{kkf})^2} (Y_{11} + Y_{22} + Y_{33})^2, \\ \dot{\omega}_{kk} &= \frac{1}{3} \dot{\omega}_{kk} = \dot{\lambda} \frac{\partial \Omega}{\partial Y_{kk}} = \frac{\dot{\lambda}}{3(\bar{\varepsilon}_{kkf})^2} Y_{kk} = \frac{\dot{\lambda}}{(\bar{\varepsilon}_{kkf})^2} Y_{kk} = \frac{\dot{\bar{\varepsilon}}_{kk}}{\bar{\varepsilon}_{kkf}} = \frac{1}{3} \frac{\dot{\bar{\varepsilon}}_{kk}}{\bar{\varepsilon}_{kkf}}.\end{aligned}\quad (20)$$

The underlined indices "kk" mean that the summation over repetitive indices is not implied, *i.e.*,  $\dot{\omega}_{kk} \neq \dot{\omega}_{11} + \dot{\omega}_{22} + \dot{\omega}_{33}$ . From these equations we may obtain the known damage parameter introduced by Kachanov (1986):  $\dot{\omega} = \dot{\omega}_{kk} = \dot{\bar{\varepsilon}}_{kk} / \bar{\varepsilon}_{kkf}$ .

For an experimental study of the damage in terms of  $\omega_1$  and  $\omega_2$  it is convenient to define  $\bar{\varepsilon}_{kk}$  and  $\bar{\varepsilon}_{eq}$  and their derivatives (*cf.*, Eqs. (19)) as material functions of the equivalent deviatoric strain  $\varepsilon_{eq}$  of the RVE, *i.e.*:

$$\bar{\varepsilon}_{kk} = \bar{\varepsilon}_{kk}(\varepsilon_{eq}), \quad \dot{\bar{\varepsilon}}_{kk} = \left[ \bar{\varepsilon}_{kk}(\varepsilon_{eq}) \right]' \frac{d\varepsilon_{eq}}{dt}, \quad \bar{\varepsilon}_{eq} = \bar{\varepsilon}_{eq}(\varepsilon_{eq}), \quad \dot{\bar{\varepsilon}}_{eq} = \left[ \bar{\varepsilon}_{eq}(\varepsilon_{eq}) \right]' \frac{d\varepsilon_{eq}}{dt}, \quad (21)$$

where the dash refers to differentiation with respect to  $\varepsilon_{eq}$ .

The technique of how the strains of both meso-elements and the RVE (which contains these meso-elements) under complex loading can be determined is outlined in Zapara *et al.* (2008). By substituting the material functions (21) into Eqs. (17) we may finally write:

$$d\omega_1 = \frac{\left[ \bar{\varepsilon}_{kk}(\varepsilon_{eq}) \right]'}{\bar{\varepsilon}_f} d\varepsilon_{eq}, \quad d\omega_2 = \frac{3}{\sqrt{2}} \frac{\left[ \bar{\varepsilon}_{eq}(\varepsilon_{eq}) \right]'}{\bar{\varepsilon}_f} d\varepsilon_{eq}. \quad (22)$$

### 3 Problem Definition and Description of the Experimental Study

#### 3.1 The problem

In order to state the particular experimental problem most concisely the differential equations of damage (22) are represented in the following integral form:

$$\omega_1 = \int_0^{\varepsilon_{eq}} \frac{\left[ \bar{\varepsilon}_{kk}(\varepsilon_{eq}) \right]'}{\bar{\varepsilon}_f(\varepsilon_{eqf})} d\varepsilon_{eq}, \quad \omega_2 = \frac{3}{\sqrt{2}} \int_0^{\varepsilon_{eq}} \frac{\left[ \bar{\varepsilon}_{eq}(\varepsilon_{eq}) \right]'}{\bar{\varepsilon}_f(\varepsilon_{eqf})} d\varepsilon_{eq}. \quad (23)$$

The determination of the material functions appearing in Eqs. (23) for as-delivered pure copper subjected to plastic deformation is the main experimental problem. The following dependencies should be experimentally investigated in order to solve this problem: the yield stress  $\sigma_y$  vs. the elongation  $\varepsilon$  of the sample, plastic dilatation  $\bar{\varepsilon}_{kk}$  of the meso-elements vs. the equivalent strain  $\varepsilon_{eq}$  of the RVE, the equivalent strain  $\bar{\varepsilon}_{eq}$  of meso-elements vs.  $\varepsilon_{eq}$ , and the limit plastic strain  $\bar{\varepsilon}_f$  of the meso-elements vs. the limit equivalent strain  $\varepsilon_{eqf}$  of the RVE.

### 3.2 Description of the experiments

The general form of the specimens with artificial defects is shown in Fig. 4. Four different types of sheet specimens made of pure copper (*Cu-0*, *Cu-1*, *Cu-2*, *Cu-3*) were prepared. One of these (*Cu-0*) has no any artificial defects while the rest has pre-machined through-holes, *i.e.*, artificial voids.

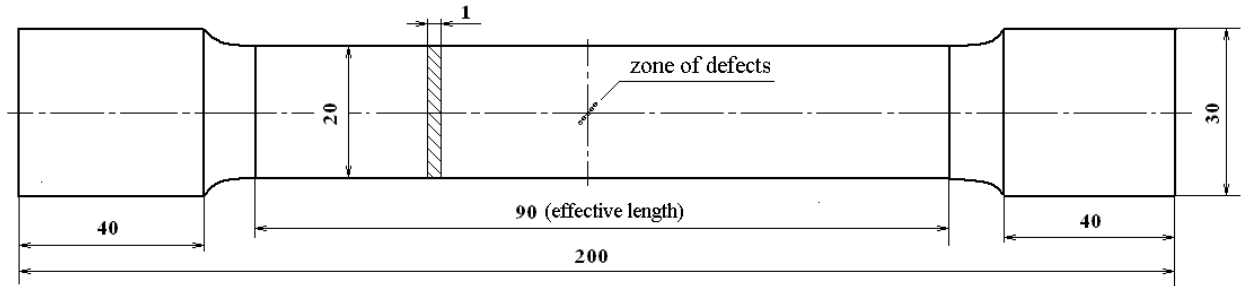


Figure 4. General form of the specimen

The zone of artificial defects (*i.e.*, an imitation of the RVE) is represented by a line of cylindrical pre-machined through-holes (of diameter  $d \cong 0.5$  mm) with different distances between the centers of the holes,  $l_c$ , and different angles  $\vartheta$  between the center line of the holes and the tensile loading direction (*cf.*, Fig. 5). The indices 1, 2, and 3 correspond to the following distances between the centers of neighboring holes:  $l_c/d = 1.5, 1.7, 1.9$ . The angles  $\vartheta$  are chosen within the range of  $\vartheta = 50 - 65^\circ$  according to the experimental hypothesis by Yokobori (1968), who revealed that large voids initiate microscopic shear bands at angles between 55-60 degree to the direction of the principal tensile stress.

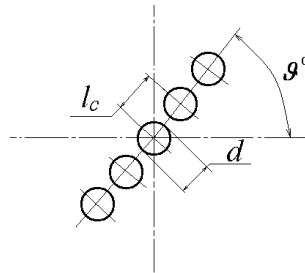


Figure 5. Arrangement of pre-fabricated holes

Specimens of each type were subjected to stepwise uniaxial tension up to fracture. The plane dimensions of the artificial voids and of the RVE were measured by means of a general-purpose optical microscope after each step of deformation while their thickness was measured by using a thickness gauge. Stepwise tension of the specimens coupled with measurements of changing defects allows us to determine the parameters of the evolution of damage during plastic deformation. Uniaxial tension was carried out in a deformation-controlled manner using a universal tensile testing machine with measurement instrumentation (*cf.*, Fig. 6) at a speed of the crossbar equal to 5 mm/min. The force of deformation  $P(t)$  and the specimen elongation  $\varepsilon = [l(t) - l_0]/l_0$ , where  $l_0, l(t)$  denote the initial and current effective length of the specimen, respectively, were measured during deformation as functions of time,  $t \in [0; t_f]$  with  $t_f$  indicating the moment of fracture. The evolution of defects within the zone of RVE was recorded by the digital camera (*cf.*, Fig. 6, *center*).



Figure 6. A specimen in the testing machine (*left*), deformation of the zone with artificial defects (*center*), measurement instrumentation (*right*)

### 3.3 Experimental data processing

#### 3.3.1 Formulation of the dependencies $\bar{\varepsilon}_{kk}(\varepsilon_{\text{eq}})$

Simple loading is realized during uniaxial tension of flat specimens (*cf.*, *e.g.*, Kachanov, 2004). The principal axes of stresses and strains coincide with the same material lines under simple loading. Hence, there is no rotation of the principal axes w.r.t. the accompanying coordinate axes which are rigidly connected to the deformed solid (*cf.*, Sedov, 1983). This fact allows us to represent the process of simple loading in the principal strain space using a line segment (*cf.*, Fig. 7) where points 0,  $M$ ,  $M_c$ , and  $M_f$  correspond to the initial, the current state of the specimen, to the onset of void coalescence, and to fracture, respectively.

The known strain path (straight-line segment  $OM_f$ ) allows us to determine the principal components  $\varepsilon_1, \varepsilon_2, \varepsilon_3$  using a rule of additive summation of strain increments:

$$\varepsilon_1 = \int_{s_{0M}} d\varepsilon_1(s) = \int_{l_{10}}^l \frac{dl_1}{l_1} = \ln \frac{l_1}{l_{10}}, \quad \varepsilon_2 = \int_{s_{0M}} d\varepsilon_2(s) = \int_{l_{20}}^{l_2} \frac{dl_2}{l_2} = \ln \frac{l_2}{l_{20}}, \quad \varepsilon_3 = \int_{s_{0M}} d\varepsilon_3(s) = \int_{l_{30}}^{l_3} \frac{dl_3}{l_3} = \ln \frac{l_3}{l_{30}}, \quad (24)$$

where  $l_{10}, l_1, l_{20}, l_2, l_{30},$  and  $l_3$  denote the linear dimensions of the RVE in the directions of the principal axes 1, 2, and 3, at the initial and current moments of tension, respectively. Note that during uniaxial tension the principal axis 1 coincides with the axial load applied to the specimen while the principal axes 2 and 3 are situated in the lateral section and axis 3 is orthogonal w.r.t. the sheet plane.

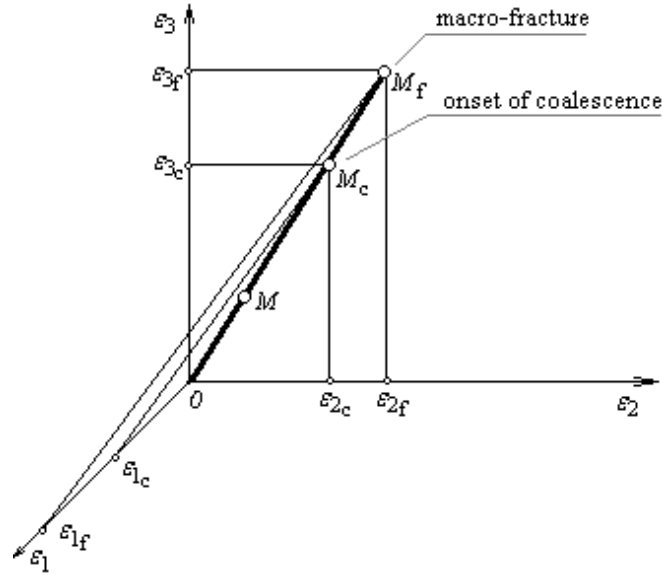


Figure 7. The strain path in the principal strain space under simple loading

Such a view on loading of a specimen allows us to determine the equivalent von Mises strain for the RVE as follows:

$$\varepsilon_{eq} = \frac{\sqrt{2}}{3} \sqrt{(\varepsilon_1 - \varepsilon_2)^2 + (\varepsilon_2 - \varepsilon_3)^2 + (\varepsilon_3 - \varepsilon_1)^2}, \quad (25)$$

where  $\varepsilon_1, \varepsilon_2, \varepsilon_3$  denote the principal components of the strain tensor.

If the linear dimensions of the RVE do not coincide with the principal axes then the principal strains should be calculated by a change in the length of material segments in the RVE in the direction of the principal axes (*cf.*, Appendix). The hypothesis about simple loading enables us to find plastic dilatation using a rule of additive summation of meso-volume increments:

$$d\bar{\varepsilon}_{kk} = \dot{\bar{\varepsilon}}_{kk} dt = \frac{\Delta \dot{V}_{ME}}{\Delta V_{ME}} dt, \quad \bar{\varepsilon}_{kk} = \int_{\Delta V_{ME0}}^{\Delta V_{ME}} \frac{d(\Delta V_{ME})}{\Delta V_{ME}} = \ln \frac{\Delta V_{ME}}{\Delta V_{ME0}}, \quad (26)$$

where  $\Delta V_{ME0}$  and  $\Delta V_{ME}$  are the meso-element volumes at the initial and current moments of deformation, respectively;  $\Delta \dot{V}_{ME}$  is the rate of a volume change in the meso-element volume.

At the initial moment of deformation the meso-element is represented by an elementary rectangular parallelepiped with sides  $\bar{l}_{10}, \bar{l}_{20}, \bar{l}_{30}$ , which coincide with the principal strain axes, and volume  $\Delta V_{ME0} = \bar{l}_{10} \bar{l}_{20} \bar{l}_{30}$ . During deformation under simple loading the meso-element transforms into a rectangular parallelepiped with the volume  $\Delta V_{ME} = \bar{l}_1 \bar{l}_2 \bar{l}_3$ . This fact allows us to present the dilatation of the meso-element as the sum of the principal strains using a rule of additive summation of strain increments:

$$\bar{\varepsilon}_{kk} = \ln \frac{\Delta V_{ME}}{\Delta V_{ME0}} = \ln \frac{\bar{l}_1 \bar{l}_2 \bar{l}_3}{\bar{l}_{10} \bar{l}_{20} \bar{l}_{30}} = \ln \frac{\bar{l}_1}{\bar{l}_{10}} + \ln \frac{\bar{l}_2}{\bar{l}_{20}} + \ln \frac{\bar{l}_3}{\bar{l}_{30}} = \bar{\varepsilon}_1 + \bar{\varepsilon}_2 + \bar{\varepsilon}_3. \quad (27)$$

If the linear dimensions of the meso-element do not coincide with the principal axes then the principal strains should be calculated by a change in the length of material segments in the meso-element in the direction of the principal axes (*cf.*, Appendix). The linear dimensions of the RVE measured at different stages of deformation allow us to find the dependence by using the relations given above.

### 3.3.2 Dependencies $\bar{\varepsilon}_{\text{eq}}(\varepsilon_{\text{eq}})$

By definition the deviatoric strain of the meso-element is given by:

$$\bar{\varepsilon}_{\text{eq}} = \frac{\sqrt{2}}{3} \sqrt{(\bar{\varepsilon}_1 - \bar{\varepsilon}_2)^2 + (\bar{\varepsilon}_2 - \bar{\varepsilon}_3)^2 + (\bar{\varepsilon}_3 - \bar{\varepsilon}_1)^2}, \quad (28)$$

In order to measure linear dimensions of the meso-element we assume the void to be inscribed into the elementary volume  $\Delta V_{ME}$  according to a geometrical model of the meso-element (*cf.*, Fig. 2). Therefore, the principal strains for meso-elements can be calculated as follows:

$$\bar{\varepsilon}_1 = \int_{s_{0M}} d\bar{\varepsilon}_1(s) = \int_{d_0}^{d_{\max}} \frac{dd}{d} = \ln \frac{d_{\max}}{d_0}, \quad \bar{\varepsilon}_2 = \int_{s_{0M}} d\bar{\varepsilon}_2(s) = \int_{d_0}^{d_{\min}} \frac{dd}{d} = \ln \frac{d_{\min}}{d_0}, \quad \bar{\varepsilon}_3 = \int_{s_{0M}} d\bar{\varepsilon}_3(s) = \int_{s_0}^s \frac{ds}{s} = \ln \frac{s}{s_0}, \quad (29)$$

where  $d_{\max}$  and  $d_{\min}$  denote the length of major and minor axis of ellipsoidal voids, respectively,  $d_0$  is the initial diameter of the cylindrical voids,  $s_0$  and  $s$  denote the thickness of the specimen in the region of the meso-element at the initial and current state of deformation, respectively.

The dimensions of meso-elements and of the RVE measured at different stages of deformation allow us to determine the strains  $\bar{\varepsilon}_{\text{eq}_k}$  and  $\varepsilon_{\text{eq}_k}$  at every  $k$ -th stage as well as the corresponding empirical dependence  $\bar{\varepsilon}_{\text{eq}}(\varepsilon_{\text{eq}})$ . Scatter of meso-element dimensions within each RVE results in scatter of their individual values ( $\hat{\varepsilon}_{kk}$  and  $\hat{\varepsilon}_{\text{eq}}$ ) at each stage of deformation. Therefore, the most probable values,  $\bar{\varepsilon}_{kk}$  and  $\bar{\varepsilon}_{\text{eq}}$ , for experimentally obtained distributions of  $\hat{\varepsilon}_{kk}$  and  $\hat{\varepsilon}_{\text{eq}}$  should be calculated for each RVE.  $\bar{\varepsilon}_{kk}$  and  $\bar{\varepsilon}_{\text{eq}}$  are the strain measures related to the  $N$ -th population of voids within the RVE. They are also the local strain characteristics of the RVE at meso-level. After processing the experimental data we have the necessary information for plotting the empirical trajectories of ductile damage in a phase plane of the meso-element strains ( $\bar{\varepsilon}_{kk}$ ,  $(3/\sqrt{2})\bar{\varepsilon}_{\text{eq}}$ ) and in a plane of the normalized parameters  $\omega_1$  and  $\omega_2$ .

## 4 Experimental Results

Fig. 8 shows experimental curves  $\sigma_y$  vs.  $\varepsilon$  obtained from the test data, where  $\sigma_y$  denotes the true yield stress at uniaxial tension and  $\varepsilon$  is the specimen elongation:  $\varepsilon = [l - l_0]/l_0$ , where  $l_0$ ,  $l$  denote the initial and current effective length of the specimen, respectively. Obviously the specimens with artificial defects ( $Cu-1$ ,  $Cu-2$ ,  $Cu-3$ ) show a limit elongation  $\varepsilon_f = 6.6-8.5\%$  which is considerably smaller than for the  $Cu-0$  specimens without artificial defects where  $\varepsilon_f = 49.8-50.0\%$ . Moreover, a decrease in the initial distance ( $l_c$ ) between neighbor artificial voids causes a decrease in the limit elongation of the specimen. For example, the specimens  $Cu-3$  ( $l_c/d = 1.9$ ) give  $\varepsilon_f = 4.9-6.5\%$  while  $\varepsilon_f = 4.3-5.7\%$  for the specimens  $Cu-1$  ( $l_c/d = 1.5$ ). An increase in the angle  $\vartheta$  results in a decrease of the limit elongation  $\varepsilon_f$  for all types of the specimens. The point  $d\sigma_y/d\varepsilon = 0$  on the curve  $\sigma_y(\varepsilon)$  corresponds to the onset of void coalescence. For the specimens without artificial defects ( $Cu-0$ ) this point is characterized by  $\varepsilon_c = 0.93\varepsilon_f$  and for the specimens  $Cu-1$ ,  $Cu-2$ , and  $Cu-3$  we have  $\varepsilon_c = (0.63 - 0.79)\varepsilon_f$ , where the lower and the upper values of  $\varepsilon_c$  refer to the specimens with  $\vartheta = 65^\circ$  and  $\vartheta = 50^\circ$ , respectively. After that coalescence evolves very fast (characterized by the falling branch of the curves  $\sigma_y(\varepsilon)$ ) and results in the initiation of the macro-crack which passes through artificial voids. The stages of the defect coalescence and the macro-crack propagation are shown in Fig. 9. During plastic tension the initially cylindrical holes-voids assume a clearly ellipsoidal shape which is elongated in the direction of the principal strain axis  $\varepsilon_1$  (*cf.*, Fig. 9).

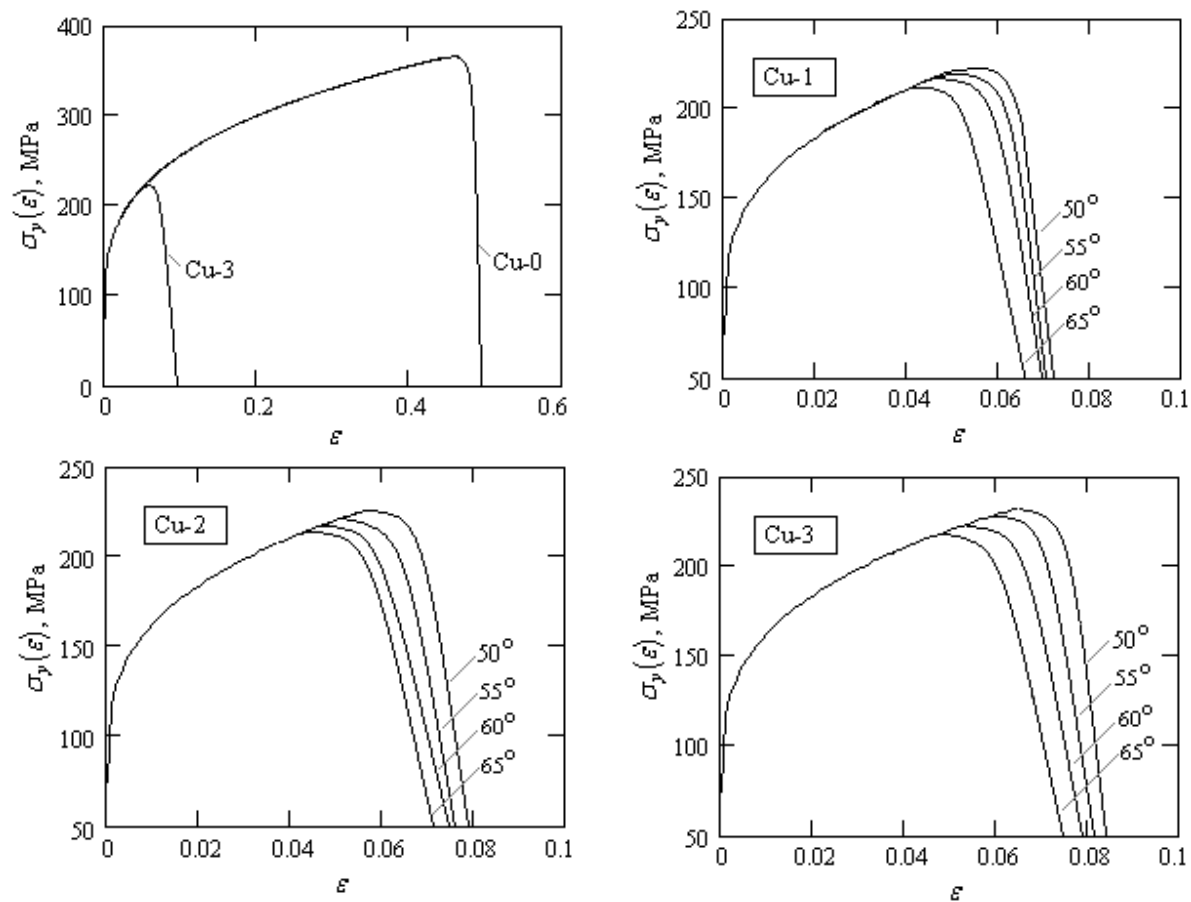


Figure 8. True yield stress at uniaxial tension,  $\sigma_y$ , vs. specimen elongation,  $\epsilon$

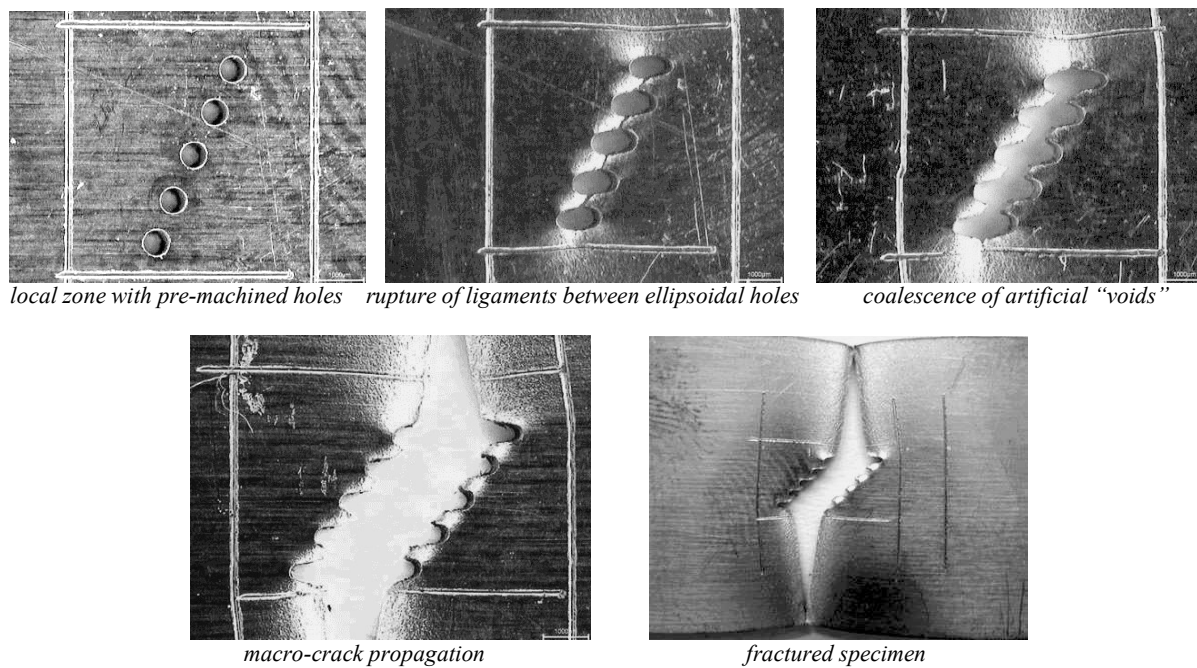


Figure 9. The main stages of damage evolution

Fig. 10 shows how the plastic dilatation of the meso-element depends on the equivalent strain of the RVE. The end point of each curve corresponds to macro-fracture of the specimen. The specimens without artificial defects reveal greater plasticity in the fracture zone ( $\varepsilon_{eq} = 0.4$ ) as compared to the specimens with artificial defects ( $\varepsilon_{eq} = 0.3-0.4$ ). The deviatoric strain  $\varepsilon_{eq_f}$  of the RVE grows due to an increase in the initial distance ( $l_c/d$ ) between neighboring cylindrical holes. The largest plastic dilatation  $\bar{\varepsilon}_{kk_f}$  of the meso-element within the fracture zone is observed in the specimens *Cu-2* at various angles  $\vartheta$ .

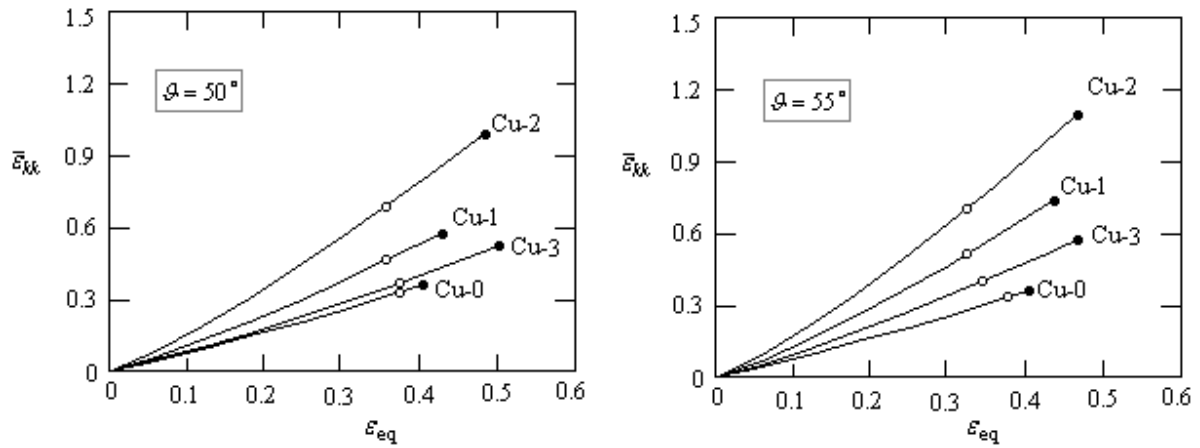
The general trend of the growing dilatation of the meso-element as it depends on the deviatoric strain of the RVE at positive stress triaxialities can be described by the following power function:

$$\bar{\varepsilon}_{kk} = b\varepsilon_{eq}^a, \quad a > 1, \quad \varepsilon_{eq} \in [0; \varepsilon_{eq_f}] \quad (30)$$

where  $a$  is a power parameter and  $b$  is a modulus of dilatation which can be determined by characteristic empirical points of the dependence  $\bar{\varepsilon}_{kk}(\varepsilon_{eq})$ , e.g., by the end point  $M_f(\varepsilon_{eq_f}; \bar{\varepsilon}_{kk_f})$  and some intermediate point  $M_1(\varepsilon_{eq_1}; \bar{\varepsilon}_{kk_1})$ :

$$a = \frac{\ln(\bar{\varepsilon}_{kk_1}/\bar{\varepsilon}_{kk_f})}{\ln(\varepsilon_{eq_1}/\varepsilon_{eq_f})}, \quad b = \frac{\bar{\varepsilon}_{kk_1}}{\varepsilon_{eq_1}^a} \equiv \frac{\bar{\varepsilon}_{kk_f}}{\varepsilon_{eq_f}^a}. \quad (31)$$

The same behavior of dilatation, *i.e.*, its increase under plastic deformation was previously revealed by Pardoen *et al.* (1998) who studied ductile fracture of copper specimens. Table 1 presents the values of the power parameter  $a$  and the modulus of dilatation  $b$  calculated by the experimental dependences  $\bar{\varepsilon}_{kk}(\varepsilon_{eq})$  for all of the investigated specimens.



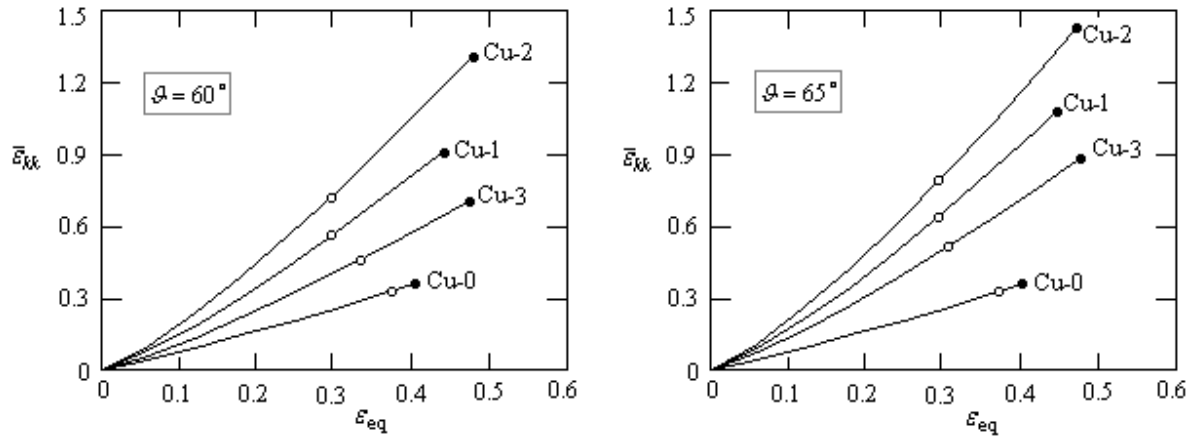


Figure 10. Plastic dilatation of the meso-element vs. the equivalent strain of the RVE  
 ○ - the point of coalescence, ● - the point of fracture

Table 1. Parameters of plastic dilatation for the test specimens

Parameters of plastic dilatation	Designation of test specimens												
	Cu-0	Cu-1				Cu-2				Cu-3			
	-	50°	55°	60°	65°	50°	55°	60°	65°	50°	55°	60°	65°
Power parameter $a$	1.240	1.222	1.123	1.149	1.216	1.202	1.194	1.227	1.164	1.311	1.110	1.331	1.253
Modulus of dilatation $b$	1.104	1.572	1.829	2.288	2.830	2.422	2.734	3.241	3.388	1.237	1.254	1.875	2.254

Fig. 11 shows the equivalent strain of the meso-element as it depends on the equivalent strain of the RVE. The end point ( $\varepsilon_{eq} = \varepsilon_{eq_f}$ ,  $\bar{\varepsilon}_{eq} = \bar{\varepsilon}_{eq_f}$ ) of the curves  $\bar{\varepsilon}_{eq}(\varepsilon_{eq})$  corresponds to the fracture. The curves  $\bar{\varepsilon}_{eq}(\varepsilon_{eq})$  can be approximated by a power function  $\bar{\varepsilon}_{eq} = \bar{b} \varepsilon_{eq}^{\bar{a}}$ , with  $\bar{a} < 1$  and  $\varepsilon_{eq} \in [0; \varepsilon_{eq_f}]$ . Since it is difficult to determine the value of  $\bar{\varepsilon}_{eq_f}$  in the moment of fracture experimentally the parameters  $\bar{a}$ ,  $\bar{b}$  can be found via the empirical point  $M_c(\varepsilon_{eq_c}; \bar{\varepsilon}_{kk_c})$  at the onset of coalescence and some intermediate point  $M_1(\varepsilon_{eq_1}; \bar{\varepsilon}_{kk_1})$ . After that the value of  $\bar{\varepsilon}_{eq_f}$  is adjusted by using the known relation  $\bar{\varepsilon}_{eq} = \bar{b} \varepsilon_{eq}^{\bar{a}}$  and the value of  $\varepsilon_{eq_f}$ . Meso-elements of the specimens Cu-1 reveal smaller equivalent strains ( $\bar{\varepsilon}_{eq_f} = 0.48 - 0.52$ ) toward the fracture when compared to the specimens Cu-2 ( $\bar{\varepsilon}_{eq_f} = 0.53 - 0.57$ ), where the lower and the upper values of  $\bar{\varepsilon}_{eq_f}$  refer to the specimens with  $\vartheta = 65^\circ$  and  $\vartheta = 50^\circ$ , respectively. The strain of the meso-element is larger than the strain of the RVE which contains these meso-elements, ( $\bar{\varepsilon}_{eq}/\varepsilon_{eq} = 1.11 - 1.28$ ), where the lower and the upper values of  $\bar{\varepsilon}_{eq}/\varepsilon_{eq}$  refer to the specimens with  $\vartheta = 65^\circ$  and  $\vartheta = 50^\circ$ , respectively.

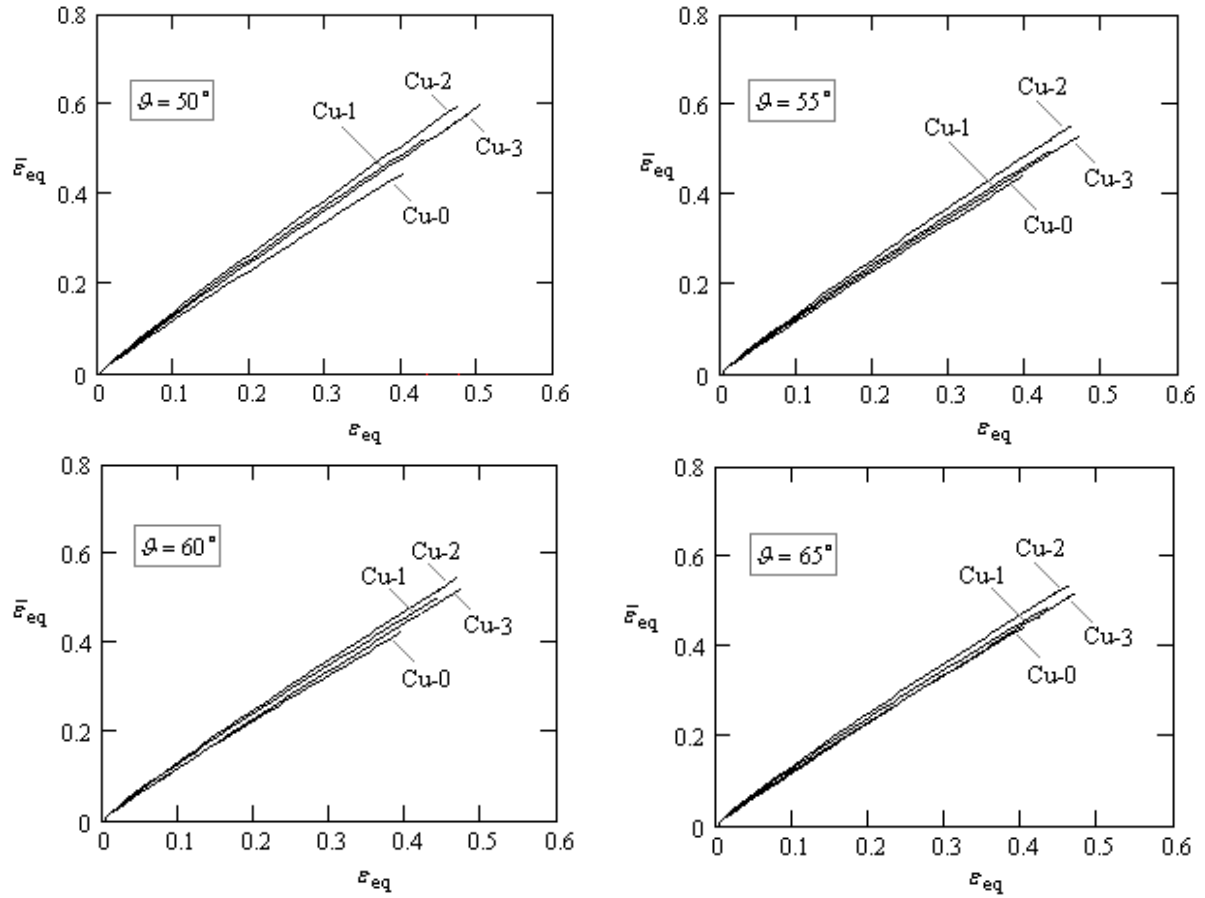


Figure 11. The equivalent strain of the meso-element vs. the equivalent strain of the RVE

The experimental dependencies  $\bar{\varepsilon}_{kk}(\varepsilon_{eq})$  and  $\bar{\varepsilon}_{eq}(\varepsilon_{eq})$  allow us to represent ductile damage of test specimens in a plane of the meso-element strains  $(3/\sqrt{2})\bar{\varepsilon}_{eq}$  vs.  $\bar{\varepsilon}_{kk}$  (cf., Fig. 12). Meso-elements with artificial voids in the specimens  $Cu-1$  reveal smaller equivalent strains  $((3/\sqrt{2})\bar{\varepsilon}_{eq_c} = 0.70-0.91)$  toward the coalescence when compared to the specimens  $Cu-3$   $((3/\sqrt{2})\bar{\varepsilon}_{eq_c} = 0.73-0.98)$ , where the lower and the upper values of  $(3/\sqrt{2})\bar{\varepsilon}_{eq_c}$  refer to the specimens with  $\vartheta = 65^\circ$  and  $\vartheta = 50^\circ$ , respectively. A small increase in the deviatoric strain  $\bar{\varepsilon}_{eq_c}$  at the coalescence is revealed due to both an increase in the initial distance between the neighboring cylindrical voids and a decrease in the angle  $\vartheta$ . The parameter  $\vartheta$  describes an effect of positional relationship between a line of defects and slip bands in ductile materials.

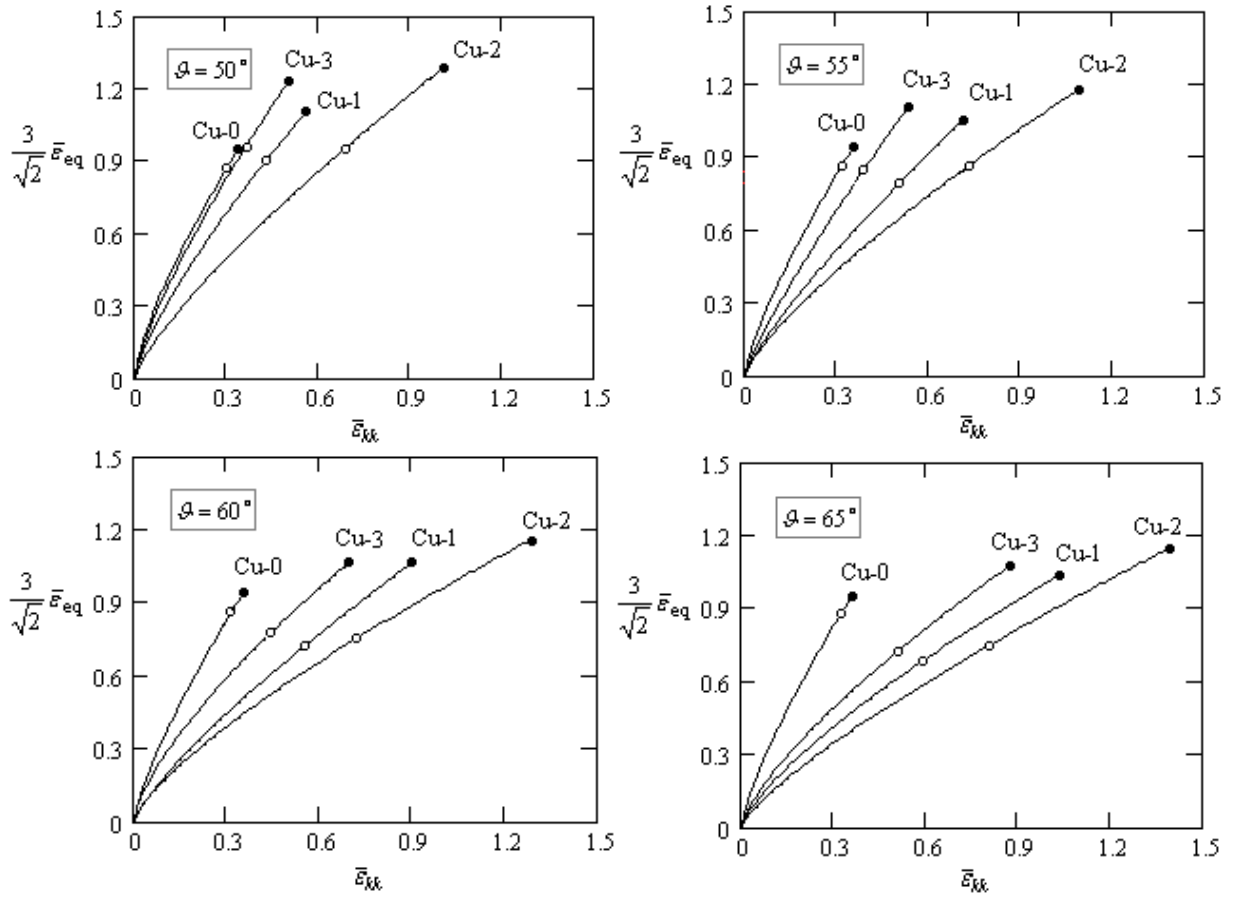


Figure 12. Representation of ductile damage of test specimens in a plane of the meso-element strains:

$$\left(\frac{3}{\sqrt{2}}\right)\bar{\varepsilon}_{eq} \text{ vs. } \bar{\varepsilon}_{kk}; \circ - \text{the point of coalescence, } \bullet - \text{the point of fracture}$$

All of the parameters of damage that appear in Eqs. (23) are now known. Fig. 13 shows trajectories of damage  $s(\omega_1, \omega_2)$  in a plane of the normalized parameters  $\omega_1$  and  $\omega_2$  calculated in the RVE zone of test specimens with artificial defects. The first four diagrams in Fig. 13 were plotted by using the experimental data obtained by the authors. The last two diagrams (Fig. 13, *bottom*) were plotted by using the experimental data by Pardoen *et al.* (1998) who studied solid and notched bars made of pure cold-drawn copper both as-delivered (left diagram) and annealed (right diagram). The trajectories  $s(\omega_1, \omega_2)$  for the specimens with holes are located more to the right as compared to those for the solid specimen  $Cu-0$ . This displacement is caused by appreciably larger plastic dilatation in the specimens with artificial defects. The onset of void coalescence in the specimens with artificial defects occurs at considerably smaller values of damage (vector magnitude:  $\omega_c = \sqrt{\omega_{1c}^2 + \omega_{2c}^2} = 0.62...0.70$ ) as compared to the solid specimens ( $\omega_c = 0.90...0.92$ ). Artificial defects substantially “prolong” a stage of coalescence and allow us to observe it during the experiment (*cf.*, Fig. 9). Trajectories  $s(\omega_1, \omega_2)$  for the specimen  $Cu-0$  and those presented by Pardoen *et al.* (1998) for as-delivered copper specimens fit satisfactorily (*cf.*, Fig. 13). Some differences seem to be caused by a spread in the properties of the as-delivered copper, specifically in the values of the limit strain  $\varepsilon_{eqf}$ . The trajectories  $s(\omega_1, \omega_2)$  for the notched specimens with higher stress triaxiality are displaced to the right w.r.t. the corresponding trajectories for the solid specimens with lower stress triaxiality. Annealed copper reveals substantially larger plasticity ( $\varepsilon_{eqf} = 0.518...0.70$ ) when compared to as-delivered copper ( $\varepsilon_{eqf} = 0.39...0.47$ ) where the lower values refer to the notched specimens with higher stress triaxiality.

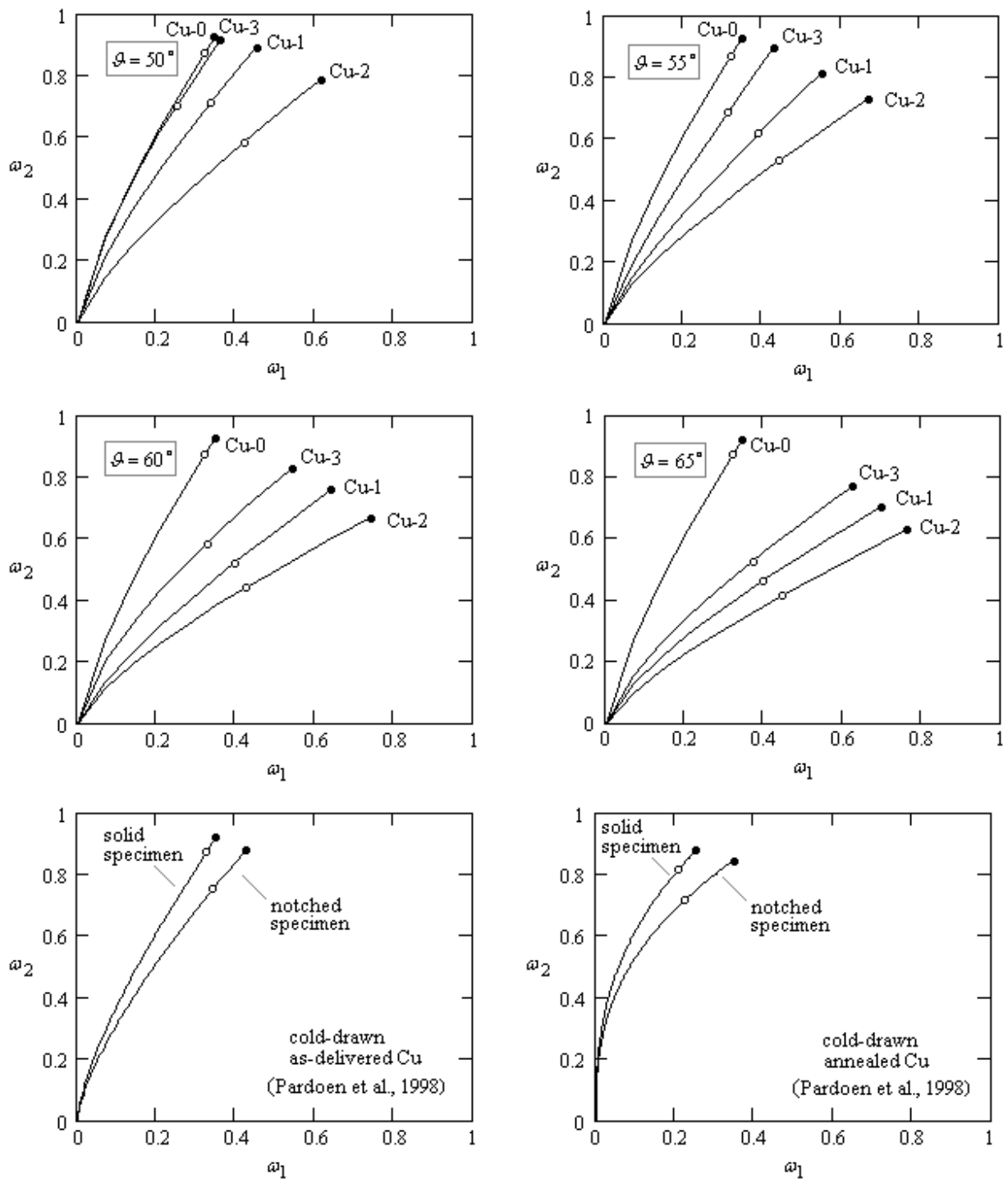


Figure 13. Trajectories  $s(\omega_1, \omega_2)$  of ductile damage in a plane of the normalized parameters  $\omega_1$  and  $\omega_2$  calculated in the fracture area of test copper specimens;  
 ○ - the point of coalescence, ● - the point of fracture

Fig. 14 shows the micro-structure of the deformed pure copper in the fracture zone of the specimen. Cavernous defects formed as a result of void coalescence and can be observed as darker local areas (the cavities of highest contrast

are indicated by white arrows). Naturally, damage induced by the strain defects is greater directly on the crack surface (Fig. 14, *center*) than around the crack (Fig. 14, *left*). Crack initiation is caused by both void coalescence and localization of the shear strains in thin slip bands.

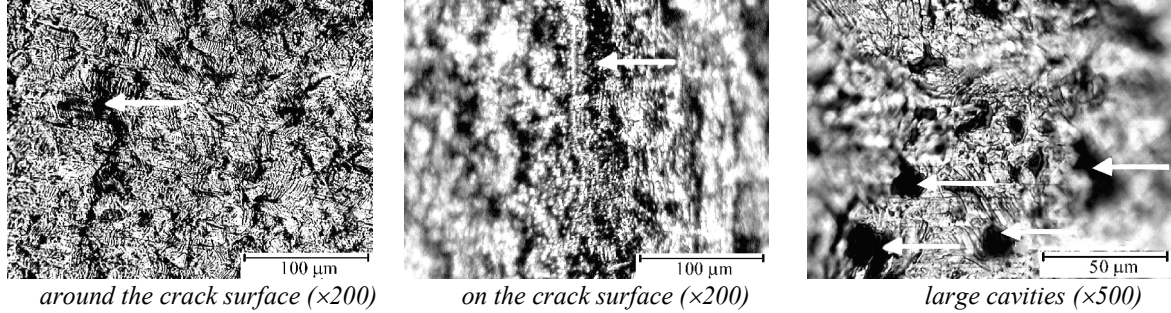


Figure 14. The micro-structure of the copper specimen after its fracture

## 5 Discussion

The main goal of the experimental research presented in this paper is to determine the material functions appearing in the constitutive relations (23) of ductile damage. The experimental technique is based on the statement that the plastic dilatation of the meso-elements (and the void volume fraction connected with it), the deviatoric strain of the RVE and of the meso-elements, as well as the functional relations between them define the measures of damage  $\omega_1$  and  $\omega_2$ .

*The dependence of plastic dilatation of the RVE on its deviatoric strain,  $\bar{\varepsilon}_{kk}(\varepsilon_{eq})$ .* The general behavior of the growth of plastic dilatation of deformed materials at positive stress triaxialities can be described by the power function (30). The power  $a > 1$  is a measure of the nonlinearity of  $\bar{\varepsilon}_{kk}(\varepsilon_{eq})$  ( $\bar{\varepsilon}_{kk}(\varepsilon_{eq})$  is linear at  $a = 1$ ). The modular parameter  $b$  describes the intensity of the growth of plastic dilatation under deformation (at  $a = 1$  the parameter  $b$  is the slope of the line  $\bar{\varepsilon}_{kk} = b\varepsilon_{eq}$ ). The dependencies of the growth of dilatation under plastic deformation, which are given in publications on ductile fracture of copper specimens (*cf.*, Pardoen *et al.*, 1998) and on the modeling of void volume fraction in ductile metals deformed at elevated temperature (*cf.*, Klöcker and Tvergaard, 2003), correspond to the same power function (30). The parameters of plastic dilatation ( $a$  and  $b$ ) are determined for all types of the test specimens (*cf.*, Table 1). The comparison of these parameters indicates that they depend on both the initial distance between voids,  $l_c$ , and on the slope angle of a line of voids,  $\vartheta$ .

*The deviatoric strain of meso-elements.* During plastic tension originally cylindrical voids assume clearly ellipsoidal shapes elongated in the direction of the principal strain axis,  $\varepsilon_1$ . The change in void shape under plastic deformation was studied by Dung (1992) and Chen *et al.* (2002). The effect of void shape on the onset of void coalescence was confirmed by Thomson *et al.* (2003). Stepwise deformation of the specimens coupled with a measurement of the RVE and meso-elements at the end of each stage is performed in order to formulate the dependence  $\bar{\varepsilon}_{eq}(\varepsilon_{eq})$ . The authors assume a simple loading scheme (*cf.*, *e.g.*, Kachanov, 2004) for the calculation of the deviatoric strains of the meso-elements ( $\bar{\varepsilon}_{eq}$ ) and of the RVE ( $\varepsilon_{eq}$ ) during uniaxial tensile tests. This approach allows us to use an additive measure for the strains in case of triaxial strain state in the fracture zone of the specimen. Such a calculation technique for the additive strains can be extended to the case of complex loading. This is very important when studying damage of metals in such tests, when the ratios between the principal strain components change under deformation (Tutyshkin *et al.*, 2001). The established dependencies  $\bar{\varepsilon}_{eq}(\varepsilon_{eq})$  indicate that the strain of the meso-element is larger than that of the RVE (which contains meso-elements). Thus the strain of the RVE is substantially averaged w.r.t. its volume. Therefore an experimental determination of the strains at meso-level is necessary in order to accurately assess damage induced by strain.

*Damage of the specimens.* Trajectories plotted in a phase plane  $(\bar{\varepsilon}_{kk}, (3/\sqrt{2})\bar{\varepsilon}_{eq})$  show the process of damage in terms of the most probable values of the meso-element strains (*cf.*, Fig. 12). Trajectories  $s(\omega_1, \omega_2)$  define the extent of damage at the present moment of deformation (via the current values of the parameters  $\omega_1$  and  $\omega_2$ ) including the onset of coalescence and the moment of fracture. The onset of void coalescence in the specimens with artificial defects occurs at considerably smaller values of damage as compared to the solid specimens. Artificial defects substantially “prolong” a stage of coalescence and allow us to observe it during the experiment (*cf.*, Fig. 9). The deviatoric strain of the RVE used as an argument in Eqs. (23) instead of the strain averaged w.r.t. the volume of the whole specimen enables us to predict the most endangered areas of the material subjected to non-uniform deformation.

Micro-defects have a strong tendency to grow and to become macro-defects. In case of large plastic strains it is appropriate to define a limit function (surface) of damage (*cf.*, Krajcinovic, 2000). The extreme points of trajectories  $s(\omega_1, \omega_2)$  belong to the failure locus (Fig. 3, *right*). The deterministic parameters of damage  $\omega_1$  and  $\omega_2$  allow us to introduce the limit function of damage (failure)  $S_f(\omega_1, \omega_2)$  which can be approximated by the Lamé curve:  $\omega_1^b + \omega_2^b = 1$ . Two damage measures  $\omega_1$  and  $\omega_2$  are required when assessing a quality of the meso-structure of metallic components produced by forming procedures (*cf.*, *e.g.*, Zapara *et al.*, 2009a; Zapara *et al.*, 2009b). It can be explained by the fact that a high-quality structure of the metal (without large cavernous defects and clusters) essentially improves an ability of components to withstand dynamic impact loads and also enhances their fatigue resistance. Such products and components are widely used in aerospace, automotive and energy engineering. The prospect of further studies in this direction is to determine trajectories of the evolution of damage for different engineering metals in a wide range of the meso-element strains typical for metal forming processes.

## Appendix

### Determination of the Principal Strains for the RVE

Here we consider the determination of the principal strains for an RVE whose outer linear dimensions do not coincide with a direction of the principal strain axes. The RVE is in the central region of the specimen (*cf.*, Fig. 4) and represented by a rectangular parallelepiped with five artificial cylindrical voids (Fig. A.1).

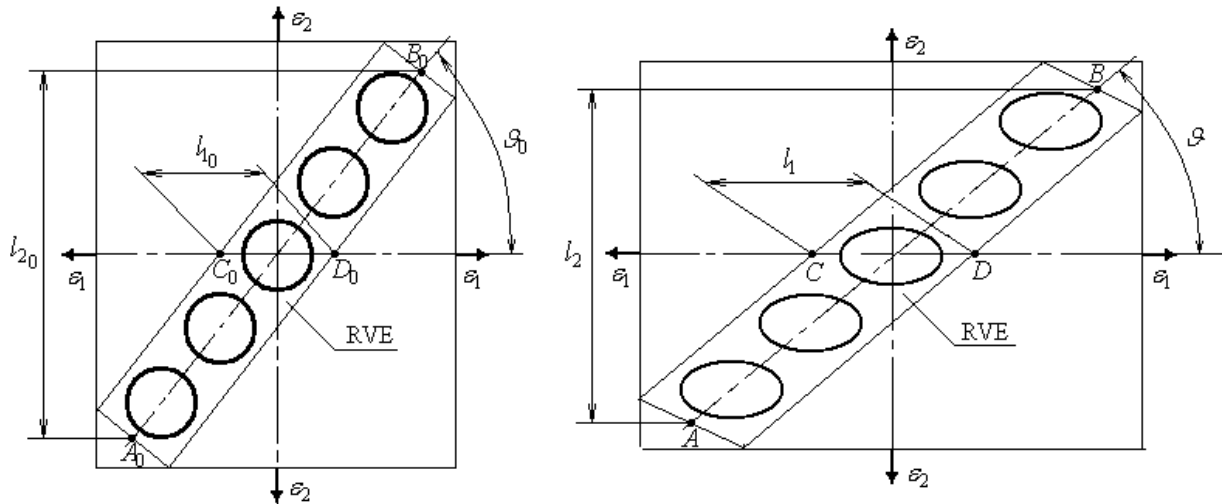


Figure A.1. The calculation model for the RVE: *left* before deformation, *right* after uniaxial tension

The direction of the first principal strain,  $\varepsilon_1$ , coincides with the tensile loading direction while the principal strains  $\varepsilon_2$  and  $\varepsilon_3$  are directed along the width and the thickness of the specimen, correspondingly. The initial position of the line of voids,  $A_0 B_0$ , w.r.t. the specimen axis (and w.r.t. the strain  $\varepsilon_1$ ) is defined by the angle  $\vartheta_0$ . During the process of deformation the RVE is transformed to a parallelepiped with ellipsoidal voids. Note that the angle between the parallelepiped edges in a sheet plane changes under deformation. The angles in the sheet thickness direction remain right as this direction coincides with the principal strain  $\varepsilon_3$  (the angular strains are equal to zero). In view of the assumed hypothesis on simple loading the principal strains of the RVE can be determined by Eqs. (24):

$$\varepsilon_1 = \int_{l_{10}}^l \frac{dl_1}{l_1} = \ln \frac{l_1}{l_{10}}, \quad \varepsilon_2 = \int_{l_{20}}^{l_2} \frac{dl_2}{l_2} = \ln \frac{l_2}{l_{20}}, \quad \varepsilon_3 = \int_{l_{30}}^{l_3} \frac{dl_3}{l_3} = \ln \frac{l_3}{l_{30}},$$

where  $l_{10} = |C_0 D_0|$ ,  $l_{20} = |A_0 B_0| \sin \vartheta_0$ ,  $l_{30} = s_0$ ,  $l_1 = |CD|$ ,  $l_2 = |AB| \sin \vartheta$ ,  $l_3 = s$ .

The material segments  $A_0 B_0$ ,  $C_0 D_0$ ,  $AB$ , and  $CD$ , as well as the angle  $\vartheta$  are measured by means of a general-purpose optical microscope while the thickness is measured by using a thickness gauge. The measurements do not reveal any noticeable curving of the initially straight material segments of the RVE. This observation confirms the known “affinity condition” for the material particle transformations during deformation (*cf.*, *e.g.*, Sedov, 1983).

**Acknowledgements** The present work was supported by Deutsche Forschungsgemeinschaft (DFG) through the research project MU 1752/25-1.

## References

- Acharya, A., Bassani, J.L.: Lattice incompatibility and a gradient theory of crystal plasticity. *J. Mech. Phys. Solids*, 48, (2000), 1565–1595
- Bonora, N., Gentile, D., Pirondi, A., Newaz, G.: Ductile damage evolution under triaxial state of stress: theory and experiments. *Int. J. Plasticity*, 21, (2005), 981-1007
- Brown, L. M., Embury, J.E.: The initiation and growth of voids at second phase particles. In: *Proc. 3rd Int. Conf. Strength of Metals and Alloys*. Institute of Metals, London, (1974), 164–169
- Brüning, M.: An anisotropic ductile damage model based on irreversible thermodynamics. *Int. J. Plasticity*, 19, (2003), 1679-1713
- Chen, B., Li, W.G., Peng, X.H.: A microvoid evolution law involving change of void shape and micro/macrosopic analysis for damaged materials. *J. Mater. Process. Techn.*, 122, (2002), 189-195
- Collins, I.F., Houlsby, G.T.: Application of thermomechanical principles to the modelling of geotechnical materials *Proc. R. Soc. Lond. A*, 453, (1997), 1975-2001
- Dung, N.L.: Plasticity theory of ductile fracture by void growth and coalescence. *Forsch. Ingenieurw.*, 58, (1992), 135-140
- Einav, I., Houlsby, G.T., Nguyen, G.D.: Coupled damage and plasticity models derived from energy and dissipation potentials. *Int. J. Solids and Structures*, 44, (2007), 2487-2508
- Fleck, N.A., Hutchinson, J.W.: Void growth in shear. *Proc. R. Soc. London, Ser. A*, 407, (1986), 435–458
- Gologanu, M., Leblond, J.B., Devaux, J.: Approximate models for ductile metals containing non-spherical voids - case of axisymmetric prolate ellipsoidal cavities. *J. Mech. Phys. Solids*, 41, (1993), 1723–1754

- Gologanu, M., Leblond, J.B., Perrin, G., Devaux, J.: Theoretical models for void coalescence in porous ductile solids. I. Coalescence in layers. *Int. J. Solids Struct.*, 38, (2001a), 5581–5594
- Gologanu, M., Leblond, J.B., Perrin, G., Devaux, J.: Theoretical models for void coalescence in porous ductile solids. II. Coalescence in columns. *Int. J. Solids Struct.*, 38, (2001b), 5595–5604
- Gurson, L.: Continuum theory of ductile rupture by void nucleation and growth. *J. Eng. Mater. Technol., Trans. ASME*, 99, (1977), 2-15
- Hammi, Y., Horstemeyer, M.F.: A physically motivated anisotropic tensorial representation of damage with separate functions for void nucleation, growth, and coalescence. *Int. J. Plasticity*, 23, (2007), 1641-1678
- Hill, R.: *The Mathematical Theory of Plasticity*. Oxford Univ. Press (1950)
- Horstemeyer, M.F., Matalanis, M.M., Sieber, A.M., Botos, M.L.: Micromechanical finite element calculations of temperature and void configuration effects on void growth and coalescence. *Int. J. Plasticity*, 16, (2000), 979-1015
- Houlsby, G.T., Puzrin, A.M.: A thermomechanical framework for constitutive models for rate-independent dissipative materials. *Int. J. Plasticity*, 16, (2000), 1017–1047
- Kachanov, L.M.: *Fundamentals of the Theory of Plasticity*. Dover Publications (2004)
- Kachanov, L.M.: *Introduction to Continuum Damage Mechanics*. Kluwer Academic (1986)
- Kannan, K., Hamilton, C.H.: Cavity distribution effects on superplastic ductility of a eutectic Pb-Sn alloy. *Scripta Mater.*, 37, (1997), 455-462
- Khraishi, T.A., Khaleel, M.A., Zbib, H.M. A parametric-experimental study of void growth in superplastic deformation. *Int. J. Plasticity*, 17, (2001), 297-315
- Klöcker, H., Tvergaard, V. Growth and coalescence of non-spherical voids in metals deformed at elevated temperature. *Int. J. Mech. Sci.*, 45, (2003), 1283–1308
- Koplik, J., Needleman, A.: Void growth and coalescence in porous plastic solids. *Int. J. Solids and Structures*, 24, (1988), 835–853
- Krajcinovic, D.: Damage mechanics: accomplishments, trends and needs. *Int. J. Solids and Structures*, 37, (2000), 267-277
- Lemaitre, J., Desmorat, R.: *Engineering Damage Mechanics: Ductile, Creep, Fatigue and Brittle Failures*. Springer (2007)
- Licht, C., Suquet, P.: Growth of cylindrical voids in nonlinear viscous material at arbitrary void volume fractions: a simple model. *Arch. Mech.*, 40, (1988), 741-757
- Magnusén, P.E., Dubensky, E.M., Koss, D.A.: The effect of void arrays on void linking during ductile fracture. *Acta Metallurgica* 36, 1503–1509 (1988)
- Makarov, E.S., Tutyshkin, N.D., Gvozdev, A.E., Tregubov, V.I., Zapara, M.A.: *Technological Mechanics of Dilating Materials*. 3rd rev. and add. edition. Tul'skiy Polygraphist Publ., Tula (2007) (in Russian)
- McClintock, F.A.: A criterion for ductile fracture by the growth of holes, *J. Appl. Mech.*, 90, (1968), 363-371

- Menzel, A., Steinmann, P.: A theoretical and computational framework for anisotropic continuum damage mechanics at large strains. *Int. J. Solids and Structures*, 38, (2001), 9505-9523
- Mulholland, M., Khraishi, T., Shen, Y.-L., Horstemeyer, M.: Void growth and interaction experiments: Implications to the optimal straining rate in superplastic forming. *Int. J. Plasticity*, 22, (2006), 1728-1744
- Needleman, A.: Void growth in an elastic plastic medium. *J. Appl. Mech.*, 39, (1972), 964-970
- Needleman, A., Tvergaard, V.: An analysis of ductile rupture in notched bars. *J. Mech. Phys. Solids*, 32, (1984), 461
- Pardoen, T., Doghri, I., Delannay, F.: Experimental and numerical comparison of void growth models and void coalescence criteria for the prediction of ductile fracture in copper bars. *Acta Mater.* 46, (1998), 541-552
- Prager, W., Hodge, P. G.: *Theory of Perfectly Plastic Solids*. New York, Wiley (1951)
- Rice, J., Tracey, D.: On ductile enlargement of voids in triaxial stress field. *J. Mech. Phys. Solids*, 17, (1969), 201-217
- Sedov, L.I.: *Continuum Mechanics*: Vol. 1. Nauka, Moscow (1983) (in Russian)
- Schacht, T., Untermann, N., Steck, E.: The influence of crystallographic orientation on the deformation behavior of single crystals containing microvoids. *Int. J. Plasticity*, 19, (2003), 1605-1626
- Stumpf, H., Makowski, J., Hackl, K.: Dynamical evolution of fracture process region in ductile materials. *Int. J. Plasticity*, 25, (2009), 995-1010
- Tait, R.A., Taplin, D.M.R.: Interaction effects during the growth of holes in a superplastically deforming medium. *Scripta Metall.*, 13, (1979), 77-82
- Thomason, P.F.: *Ductile Fracture of Metals*. Pergamon Oxford (1990)
- Thomson, C.I.A.; Worswick, M.J.; Pilkey, A.K.; Lloyd, D.J.: Void coalescence within periodic clusters of particles. *J. Mech. Phys. Solids*, 51, (2003), 127-146
- Tracey, D.M.: Strain hardening and interaction on the growth of voids in ductile fracture. *Eng. Fract. Mech.*, 3, (1971), 301-316
- Tutyshkin, N.D., Gvozdev, A.E., Tregubov, V.I., Poltavets, Y.V., Selyodkin, E.M., Pustovgar, A.S.: *Complex Problems of the Plasticity Theory*. Tul'skiy Polygraphist, Tula (2001) (in Russian)
- Tvergaard, V., Niordson, C.: Non local plasticity effects on interaction of different size voids. *Int. J. Plasticity*, 20, (2004), 107-120
- Voyiadjis, G.Z., Dorgan, R.J.: Framework using functional forms of hardening internal state variables in modeling elasto-plastic-damage behavior. *Int. J. Plasticity*, 23, (2007), 1826-1859
- Weck, A., Wilkinson, D.S.: Experimental investigation of void coalescence in metallic sheets containing laser drilled holes. *Acta Materialia*, 56, (2008), 1774-1784
- Weck, A., Wilkinson, D.S., Maire, E., Toda, H.: Visualization by X-ray tomography of void growth and coalescence leading to fracture in model materials. *Acta Materialia*, 56, (2008), 2919-2928
- Yokobori, T.: *An Interdisciplinary Approach to Fracture and Strength of Solids*. Gordon & Breach, Pub. New York (1968)

Zapara, M.A., Tutyshkin, N.D., Müller, W.H., Weinberg, K., Wille, R.: A physico-mechanical approach to modeling of metal forming processes – Part I: Theoretical framework. *Cont. Mech. Therm.*, 20 (4), (2008), 231-254

Zapara, M.A., Tutyshkin, N.D., Müller, W.H., Weinberg, K., Wille, R.: A physico-mechanical approach to modeling of metal forming processes – Part II: damage analysis in processes with plastic flow of metals. *Cont. Mech. Therm.*, 20 (8), (2009a), 509-521

Zapara, M.A., Tutyshkin, N.D., Müller, W.H., Wille, R.: Analysis of processes with axisymmetric plastic flow of metals. *Technische Mechanik*, 29 (2), (2009b), 87-114

Zapara, M.A., Tutyshkin, N.D., Müller, W.H., Wille, R.: Experimental study and modeling of damage of Al alloys using tensor theory. *Cont. Mech. Therm.*, 22 (2), (2010), 99-120

Zhang Z.L., Hauge M.: On the Gurson micromechanical parameters. *Fatigue and Fracture Mechanics*, 29, (1990), 364-383

---

*Addresses:*

Prof. Dr. W.H. Müller, Dr. R. Wille, and Dr. M. Zapara, Lehrstuhl für Kontinuumsmechanik und Materialtheorie, Technische Universität Berlin, Sekretariat MS 02, Einsteinufer 5, D-10587 Berlin, Germany.

E-mail: Wolfgang.H.Mueller@tu-berlin.de, Ralf.Wille@tu-berlin.de, Maksim.Zapara@tu-berlin.de

Prof. Dr. N. Tutyshkin, Lehrstuhl für Technische Mechanik, Universität Tula, 300600 Tula, Russland.

E-mail: tutyshkin@mail.ru